

High concentrations of sub-3nm clusters and frequent new particle formation observed in the Po Valley, Italy, during the PEGASOS 2012 campaign

J. Kontkanen¹, E. Järvinen^{1,2}, H. E. Manninen¹, K. Lehtipalo^{1,3}, J. Kangasluoma¹, S. Decesari⁴, G. P. Gobbi⁵, A. Laaksonen^{6,7}, T. Petäjä¹, and M. Kulmala¹

[1]{Department of Physics, 00014 University of Helsinki, Helsinki, Finland}

[2]{Institute for Meteorology and Climate Research, Karlsruhe Institute of Technology, 76021 Karlsruhe, Germany}

[3]{Paul Scherrer Institute, 5232 Villigen PSI, Switzerland}

[4]{Istituto di Scienze dell'Atmosfera e del Clima, CNR, 40129 Bologna, Italy}

[5]{Institute of Atmospheric Sciences and Climate, CNR, 00133 Rome, Italy }

[6]{Department of Applied Physics, University of Eastern Finland, 70211 Kuopio, Finland}

[7]{Finnish Meteorological Institute, 00101 Helsinki, Finland}

Correspondence to: J. Kontkanen (jenni.kontkanen@helsinki.fi)

Abstract

The concentrations of neutral and charged sub-3nm clusters and their connection to new particle formation (NPF) were investigated during the PEGASOS campaign (7 June – 9 July, 2012) at the San Pietro Capofiume measurement station in the Po Valley, Italy. Continuous high concentrations of sub-3nm clusters were detected during the measurement period, although the condensation sink was relatively high (median value $1.1 \times 10^{-2} \text{ s}^{-1}$). The median cluster concentrations were 2140 cm^{-3} and 7980 cm^{-3} in the size bins of 1.5–1.8 nm and 1.8–3 nm, and the majority of them were electrically neutral. NPF events were observed during the measurement period frequently, on 86% of the days. The median growth rates of clusters during the events were 4.3 nm h^{-1} , 6.0 nm h^{-1} and 7.2 nm h^{-1} in the size ranges of 1.5–3 nm, 3–7 nm and 7–20 nm. The median formation rate of 1.6 nm clusters was high, $45 \text{ cm}^{-3} \text{ s}^{-1}$, and it

1 exceeded the median formation rate of 2 nm clusters by one order of magnitude. The ion-
2 induced nucleation fraction was low; the median values were 0.7% at 1.6 nm and 3.0% at 2 nm.
3 On NPF event days the neutral cluster concentration had a maximum around 9 a.m. (local winter
4 time), which was absent on a non-event day. The increase in the cluster concentrations in the
5 morning coincided with the increase in the boundary layer height. At the same time radiation,
6 temperature and SO₂ concentration increased, and RH and condensation sink decreased. The
7 concentrations of neutral and charged clusters were observed to have a positive correlation with
8 sulfuric acid proxy, indicating the significance of sulfuric acid for the cluster formation in San
9 Pietro Capofiume. The condensation sink had a negative correlation with the concentration of
10 charged clusters but no clear relation to the neutral cluster concentration. This finding, together
11 with back-trajectory analysis, suggests that the precursor vapors of the clusters and background
12 aerosol particles, acting as their sink, have possibly originated from the same sources, including
13 e.g. power plants and industrial areas in the Po Valley.

14

15 **1 Introduction**

16 New particle formation (NPF) is a dominant source of aerosol particles in the atmosphere
17 (Spracklen et al. 2006; Yu et al., 2010). The process takes place by the formation of nanometer-
18 sized atmospheric clusters and their subsequent growth to larger particles (Kulmala et al., 2007;
19 2013). After that they may affect the climate through indirect radiative effects of aerosol
20 particles (Merikanto et al., 2009; Wang and Penner, 2009; Kazil et al., 2010; Makkonen et al.,
21 2012). NPF has been observed around the world in various locations (Kulmala et al., 2004a;
22 Zhang et al., 2012). Although recent chamber studies have provided insight into the role of
23 different chemical compounds in NPF (Kirkby et al., 2011; Almeida et al., 2013; Schobesberger
24 et al. 2013; Riccobono et al., 2014), the exact mechanisms, by which the process takes place in
25 different ambient conditions, are still unknown. The summary of the recent knowledge on
26 physical and chemical processes behind NPF is given by Kulmala et al. (2014).

27 The relative importance of electrically neutral and charged clusters in atmospheric NPF has
28 been under discussion for decades. Some model studies underline the importance of ions (Yu
29 and Turco, 2000; Yu and Turco, 2008), while field measurements conducted with ion
30 spectrometers suggest only a minor contribution of ions to NPF in the continental boundary
31 layer (Iida et al., 2006; Kulmala et al., 2007; Manninen et al., 2010) and also higher in the
32 troposphere (Mirme et al., 2010). Recent instrumental development has enabled measuring the

1 concentrations of sub-3nm particles also with condensation particle counters, including a
2 Particle Size Magnifier (PSM; Vanhanen et al., 2011). With these measurement techniques, it
3 has been observed that sub-3nm neutral clusters exist in boreal forest (Lehtipalo et al. 2009;
4 Kulmala et al., 2013), in coastal areas (Lehtipalo et al., 2010), and at high altitude under free
5 tropospheric conditions (Rose et al., 2015). At all these sites, the concentrations of neutral
6 clusters clearly exceed ion concentrations during NPF, which indicates that neutral nucleation
7 mechanisms dominate in these environments. Furthermore, high concentrations of sub-3nm
8 clusters during NPF events have been detected with a PSM at urban sites in the United States
9 (Yu et al., 2014) and at urban, heavily polluted, sites in China (Xiao et al., 2015; Yu et al.,
10 2015).

11 In many of the earlier studies, sub-3nm clusters detected with a PSM have been observed to be
12 associated with elevated sulfuric acid concentration (Kulmala et al., 2013; Yu et al., 2014). This
13 indicates that sulfuric acid is a key compound in the formation of atmospheric clusters, as has
14 been proposed already earlier (e.g. Weber et al., 1997; Sipilä et al., 2010). Sulfuric acid is
15 formed in the atmosphere by the oxidation of sulfur dioxide (SO₂), which is largely produced
16 in fossil fuel combustion. Therefore, anthropogenic emissions of SO₂ may enhance the
17 formation of sub-3nm clusters. On the other hand, high aerosol surface area related to
18 anthropogenic emissions may reduce the sub-3nm cluster concentrations by coagulation
19 (Kerminen et al., 2001; Xiao et al., 2015). Besides sulfuric acid, organic compounds with very
20 low volatility may participate in atmospheric cluster formation (Kulmala et al., 1998; Metzger
21 et al., 2010; Ehn et al., 2014; Schobesberger et al., 2013; Riccobono et al., 2014). These
22 compounds are formed in the atmosphere in the oxidation of VOCs (volatile organic
23 compounds), mainly originating from biogenic sources, such as vegetation (Günther et al.,
24 2012).

25 In addition to the concentrations of low-volatile precursor vapors, meteorological conditions
26 may influence the sub-3nm cluster concentrations. Local meteorology can affect cluster
27 concentrations in several ways. For instance, solar radiation drives oxidation mechanisms
28 forming low-volatile vapors, which, as mentioned above, may participate in the formation of
29 clusters. This is indicated by numerous observations on the importance of solar radiation for
30 NPF (e.g. Boy et al., 2002; Nieminen et al., 2015). In addition, NPF has been observed to be
31 more favorable in the boundary layer when relative humidity and background aerosol
32 concentrations are low (Hyvönen et al., 2005; Hamed et al., 2011; Nieminen et al., 2015). It has

1 also been proposed that the beginning of NPF may be linked to the onset of turbulence in the
2 boundary layer (Nilsson et al, 2001a). In addition, the origin of air masses has been connected
3 to the probability of NPF events in several locations (Nilsson et al., 2001b; Sogacheva et al.,
4 2007; Nieminen et al., 2015).

5 In this study, we investigated the concentrations of sub-3nm clusters at the San Pietro
6 Capofiume station located in the Po Valley, Italy, during the PEGASOS campaign (7 June – 9
7 July, 2012). Previously, NPF events have been found to be frequent in San Pietro Capofiume
8 during summer (Laaksonen et al., 2005; Hamed et al., 2007; Manninen et al., 2010), which may
9 be due to the high emissions of anthropogenic precursor vapors and favorable meteorological
10 conditions. Here, our aim is to further investigate NPF occurring at this site focusing on the
11 concentrations of sub-3nm clusters and their connection to NPF events. Furthermore, we aim
12 to elucidate the effect of meteorological conditions and the presence of anthropogenic pollutants
13 on the sub-3nm cluster concentrations in San Pietro Capofiume. During the campaign, the
14 concentration of all sub-3nm clusters were measured with a PSM and the concentration of
15 charged clusters with a NAIS (Neutral cluster and Air Ion Spectrometer; Kulmala et al., 2012).
16 From these measurements, we determined the growth rates and formation rates of clusters. We
17 compared the diurnal variation of cluster concentrations and their formation rates to the diurnal
18 evolution of planetary boundary layer and the variation of different meteorological variables.
19 In addition, we studied how the sulfuric acid concentration and condensation sink as well as the
20 origin of air masses affect the concentrations of sub-3nm clusters observed in San Pietro
21 Capofiume.

22

23 **2 Measurements and data analysis**

24 **2.1 Site description and instrumentation**

25 The measurements took place at the San Pietro Capofiume meteorological station in northern
26 Italy (44° 39'N, 11° 37'E, 11 m a.s.l) during 7 June – 9 July 2012. The measurements were part
27 of the PEGASOS (Pan-European Gas–Aerosol–Climate Interaction Study) Zeppelin campaign
28 where San Pietro Capofiume was one of the ground stations. The meteorological station is
29 located about 30 km northeast from the city of Bologna in the Po Valley (Fig. 1). The Po Valley
30 region is situated between the Alps in the north and the Apennines Mountains in the south-
31 southwest. The mountains surround the valley on three sides and strongly modify both the local
32 and regional air flow patterns in the area (Sogacheva et al., 2007). High levels of anthropogenic

1 pollutants have been observed in the region due to the emissions from power plants and
2 industrial areas. In addition, the emissions from ship traffic in the Adriatic Sea (Hamed et al.,
3 2007) and long-range transport from Central and Eastern Europe are possible sources of
4 pollutants in the region (Sogacheva et al., 2007).

5 During the measurement campaign, the total particle concentrations were measured with an
6 Airmodus Particle Size Magnifier (PSM A09; Vanhanen et al., 2011). PSM is a dual-stage
7 mixing-type condensation particle counter. In the first stage, diethylene-glycol is used to
8 activate and grow the particles to about 90 nm in diameter, after which the further growth and
9 the counting of particles is done with a conventional CPC. The cut-off size of the PSM can be
10 changed by altering the mixing ratio of the sample and saturator flow. In this study, the cut-off
11 sizes of 1.5 nm and 1.8 nm were used, and thus, the total concentration of clusters in the size
12 range of 1.5–1.8 nm was obtained. These cut-off sizes were determined based on laboratory
13 calibrations using ammonium sulphate particles produced in a tube furnace. It needs to noted,
14 though, that the cut-off size of the PSM has been observed to depend on environmental
15 conditions, especially on relative humidity, and on the composition and the charge of clusters
16 (Kangasluoma et al., 2013; Wimmer et al., 2013). Therefore, the cut-off sizes obtained in the
17 laboratory may not correspond exactly to the cut-off sizes of the instrument in field
18 measurements.

19 In addition, a twin-DMPS (Differential Mobility Particle Sizer) system was used to measure
20 the number size distribution of particles in the size range of 3–600 nm (Aalto et al., 2001;
21 Laaksonen et al., 2005). By subtracting the concentration measured with the highest cut-off size
22 of the PSM from the total particle concentration measured with the DMPS, we obtained the
23 total concentration of clusters and particles in the size range of 1.8–3 nm. Furthermore, the
24 number size distributions of positive and negative ions between 0.8 and 42 nm and the number
25 size distributions of all particles between 2 and 42 nm were measured with a Neutral Cluster
26 and Air Ion Spectrometer (NAIS; Kulmala et al., 2012; Mirme and Mirme, 2013). By
27 interpolating the NAIS data, the ion concentrations in the 1.5–1.8 nm and 1.8–3.0 nm size
28 ranges were obtained. However, the NAIS was not working properly in ion mode during 11–
29 21 June, and therefore this period was excluded from the analysis.

30 In addition to particle size distribution data, meteorological data, including temperature, relative
31 humidity and global radiation, measured at the station were used in the analysis. The data
32 obtained with a SO₂ monitor (model 43i-TLE, Thermo Scientific) were also utilized.

1 Furthermore, the measurement station was equipped with a ceilometer (Jenoptik CHM15K),
2 which allowed us to monitor the evolution of planetary boundary layer (PBL; Di Giuseppe et
3 al., 2012; Angelini and Gobbi, 2014).

4

5 **2.2 Determining the concentration of neutral clusters**

6 To study the importance of ion-mediated processes for cluster formation, we calculated the
7 number of neutral clusters originating from the collisions between oppositely charged ions, i.e.
8 recombination products, in the size bins of 1.5–1.8 nm and 1.8–3 nm. The concentration of
9 recombination products in size bin i was obtained from (Kontkanen et al., 2013):

$$10 \quad N_{rec,i} = \frac{\lambda_i \alpha \sum_{j,k} r_{ijk} N_j^+ N_k^-}{CoagS_i}. \quad (1)$$

11 Here λ_i represents the fraction of stable recombination products that do not break up instantly
12 after their formation in size bin i . α is the ion–ion recombination coefficient for which we used
13 the value of $1.6 \times 10^{-6} \text{ cm}^3 \text{ s}^{-1}$ (Hoppel and Frick, 1986; Tammet and Kulmala, 2005). N_j^+ and
14 N_k^- refer to the concentrations of positive and negative ions in size ranges j and k , respectively,
15 and r_{ijk} tells how large fraction of the recombination products formed in their collisions end up
16 in size bin i . $CoagS_i$ is the average coagulation sink for size range i . Thus, Eq. (1) takes into
17 account the production of neutral clusters in the collisions between two oppositely charged ions
18 (the term in the numerator) and their loss by coagulation (the term in the denominator). The
19 effect of the condensational growth of clusters was neglected, as has been done in most of the
20 earlier studies discussing the concentrations of recombination products (e.g. Lehtipalo et al.,
21 2009; Kulmala et al., 2013). The production rate of neutral clusters due to ion-ion
22 recombination was calculated from the ion size distribution measured with the NAIS. For the
23 detailed description of the procedure, see Kontkanen et al. (2013). The fraction of stable
24 recombination products, λ_i , was assumed to equal unity. The coagulation loss of clusters
25 because of their collisions onto larger aerosol particles was calculated from DMPS data
26 (Kulmala et al., 2001).

27 After calculating the concentration of recombination products, we calculated the concentration
28 of neutral clusters ($N_{n,i}$), not originating from ion-ion recombination (from now on we refer to
29 these as just neutral clusters), in the size bins of 1.5–1.8 nm and 1.8–3 nm by subtracting the

1 concentrations of ions ($N_{ions,i}$) and recombination products ($N_{rec,i}$) from the total cluster
2 concentration ($N_{tot,i}$):

$$3 \quad N_{n,i} = N_{tot,i} - N_{ions,i} - N_{rec,i} \quad (2)$$

4 For calculating the concentration of neutral clusters from Eq. (2) 10-minute averaged data from
5 the NAIS ($N_{ions,i}$), and from the PSM and the DMPS ($N_{tot,i}$) were used.

6

7 **2.3 New particle formation event analysis**

8 The classification of measurement campaign days into new particle formation (NPF) event days
9 and non-event days was done by visually evaluating ion size distribution data from the NAIS
10 (Dal Maso et al., 2005; Hirsikko et al., 2007). The days when new particle formation and growth
11 were observed were classified as NPF event days, while the days with no implication of NPF
12 were assigned as non-event days.

13 The growth rates of 1.5–3 nm, 3–7 nm and 7–20 nm particles were determined for the identified
14 NPF events. For calculating the growth rates, we used positive ion size distribution data
15 measured with the NAIS and applied the method by Hirsikko et al. (2005). In this method a
16 Gaussian distribution is fitted to the concentration time series at a certain size to determine the
17 moment of maximum concentration. Then, the growth rate is obtained as the slope of a linear
18 least square fit to the moments of maximum concentrations and the corresponding geometric
19 mean diameters of the particles. For the comparison of particle growth rates determined using
20 different instruments and methods, see Yli-Juuti et al. (2011).

21 The total particle formation rates and ion formation rates at 1.6 nm ($J_{1.6}$) and at 2 nm (J_2) were
22 calculated following the method in Kulmala et al. (2012). When calculating the total particle
23 formation rate, we determined the time derivative of particle concentration and took into
24 account the effects of coagulation loss and the growth out of the studied size range. The
25 accuracy of this method is evaluated in Korhonen et al. (2011). When determining the ion
26 formation rate, the loss of ions by ion-ion recombination and the charging of neutral particles
27 were also included in the calculation. The total particle formation rate at 1.6 nm was determined
28 from the PSM data, while for calculating the total particle formation rate at 2 nm we used NAIS
29 particle size distribution data. The ion formation rates were calculated from the NAIS ion size
30 distributions. For the growth rates needed for the calculations, we used the growth rates
31 determined for 1.5–3 nm size range from the NAIS data. However, it needs to be noted that the

1 growth rates of neutral and charged clusters may not be equal in reality, as the presence of
2 charge may enhance the growth of particles (e.g. Yu and Turco, 2000; Nadykto and Yu, 2003).

3

4 **2.4 Sulfuric acid proxy**

5 To study the connection between the concentrations of sub-3nm clusters and sulfuric acid, we
6 calculated the sulfuric acid concentration from a non-linear statistical proxy derived by
7 Mikkonen et al. (2011):

$$8 \quad SA_{\text{proxy}} = 8.21 \times 10^{-3} \times k \times \text{Rad} \times [\text{SO}_2]^{0.62} \times (\text{CS} \times \text{RH})^{-0.13} \quad (3)$$

9 Here k describes the reaction rate coefficient, which depends on air temperature and
10 atmospheric pressure. Rad refers to global radiation, $[\text{SO}_2]$ to the concentration of sulfur
11 dioxide and RH to relative humidity. CS is the condensation sink that we calculated from the
12 particle size distributions measured with the DMPS assuming that the condensing vapor is
13 sulfuric acid, and correcting for the hygroscopic growth of particles (Kulmala et al., 2001;
14 Laakso et al., 2004). The proxy was calculated only for times when global radiation exceeded
15 10 W m^{-2} . Mikkonen et al. (2011) concluded that their proxy is suitable for estimating sulfuric
16 acid concentration in a wide range of environmental conditions. Still, as there were no
17 measurements of sulfuric acid concentration during our measurement campaign, the accuracy
18 of the proxy in these specific conditions could not be assessed.

19

20 **2.5 Trajectory analysis**

21 To investigate the origin of air masses during the measurement campaign, we calculated 24-
22 hour backward trajectories using the HYSPLIT (Hybrid Single-Particle Lagrangian Integrated
23 Trajectory) model (Draxler and Rolph, 2015). Global FNL (Final) meteorological archive
24 generated by the NCEP GDAS (National Centers for Environmental Prediction Global Data
25 Assimilation System) were used in the calculations. For each day we studied trajectories
26 arriving at the measurement site hourly between 10 a.m. and 2 p.m. local winter time (UTC +
27 1 h) with the arrival height of 100 m. We determined the arrival direction of the air mass by
28 dividing the trajectories into 22.5° sectors. If a trajectory spent over 70% of the last 24 h before
29 arriving to San Pietro Capofiume in a certain sector, that sector was selected to correspond to
30 the arrival direction of the air mass.

31

1 **3 Results and discussion**

2 **3.1 Meteorological conditions in San Pietro Capofiume during the PEGASOS** 3 **campaign**

4 The weather conditions during the campaign were initially characterized by moderate instability
5 (from 8th to 14th June), which was followed by a series of sunny, hot days with relative
6 humidity (RH) decreasing from day to day. The mean temperature for the campaign (25.5°C)
7 was 3.5°C higher compared to a 15-year climatology for the site (data from the Regional
8 Agency for Environmental Protection, ARPA, of Emilia-Romagna). The average RH was 16%
9 lower than typically, and the cumulated rain (24 mm) was half of the expected amount. In
10 summary, the ambient conditions during the experiment were more representative for a heat-
11 wave period than for an average summer in the Po Valley.

12 The meteorological conditions prevailing during the campaign resulted in the strong diurnal
13 variation of radiation, temperature and RH. The diurnal cycles of these variables are presented
14 in Fig. 2 for new particle formation (NPF) event days (86% of the days, see Sect. 3.3) and the
15 only non-event day (6 July 2012) in local winter time (UTC + 1 h). For NPF event days the
16 median diurnal cycle and the 25% to 75% percentile range are shown. On NPF event days
17 global radiation started typically increase around 4 a.m. in the morning, and reached its
18 maximum (median value 940 W/m²) at noon (Fig. 2a). Temperature began to increase from its
19 night-time values (about 20 °C) at the same time with the radiation and was highest (about 33
20 °C) around 3 p.m. (Fig. 2b). The diurnal cycle of RH was opposite to that of temperature: RH
21 was highest (about 84 %) early in the morning and lowest (about 30%) in the afternoon (Fig.
22 2b). On the non-event day global radiation increased in the morning slightly slower than
23 typically on event days, and after reaching its maximum (820 W/m²) around noon the radiation
24 level dropped rapidly. Correspondingly, temperature also decreased in the afternoon being at
25 that time 6–8 °C lower than typically on NPF event days. On the other hand, in the morning of
26 the non-event day temperature was similar, or even slightly higher, than typically on event days.
27 Furthermore, starting from 6 a.m. RH was higher on the non-event day than on event days,
28 exceeding 60% in the afternoon. The results support previous studies from San Pietro
29 Capofiume where NPF events have been observed to occur on days with high solar radiation
30 and low RH (Hamed et al., 2007; Sogacheva et al., 2007).

31 Figure 2a also presents the diurnal variation of PBL height. On NPF event days the progressive
32 increase of the mixing layer from about 250 m to 1 700 m can be observed between 7 a.m. and

1 3 p.m. Therefore, the first steps of the photochemical processes observed at the station were
2 triggered by reactions occurring in a rather thin atmospheric surface layer. Conversely, in the
3 late morning and in the afternoon hours, the thickness of the PBL was great enough to allow
4 the entrainment of air masses with their burden of chemical compounds travelling over long
5 distances. On the non-event day the PBL height increased higher than typically on event days
6 reaching about 2000 m. However, similarly as radiation, the PBL height quickly decreased in
7 the afternoon being at that time about 1000 m lower than the PBL height typically on event
8 days. Further analysis of ceilometer data reveals that low-level clouds were present in the
9 morning and rainfall occurred between 2 p.m. and 3 p.m. on the non-event day, which explains
10 the observed behavior of radiation, RH and the PBL height.

11 The effect of PBL height on background aerosol concentrations can be seen in the median
12 diurnal variation of condensation sink (Fig. 2c). Condensation sink was highest around 2 a.m.
13 when boundary layer was still thin. The maximum value of condensation sink was higher on
14 the non-event day (0.023 s^{-1}) than typically on NPF event days (median value 0.015 s^{-1}). During
15 the early morning, when the PBL started to form, condensation sink rapidly decreased and
16 around 9 a.m. reached its daytime level (about 0.01 s^{-1} both on NPF event days and on the non-
17 event day). During the day, when mixing layer extended higher in the atmosphere, condensation
18 sink stayed low starting to increase again after 6 p.m. Our observation on the lower
19 condensation sink in the mornings of NPF event days compared to the non-event day is
20 consistent with Hamed et al. (2007), who showed that low condensation sink favor particle
21 formation in San Pietro Capofiume.

22 The diurnal patterns of SO_2 concentration and sulfuric acid proxy were also slightly different
23 on NPF event days and on the non-event day (Fig 2d). On event days SO_2 concentration started
24 to rise from its low night-time values (median value 0.13 ppb) around 5 a.m. reaching its
25 maximum (about 0.9 ppb) around 9 a.m. After that SO_2 concentration decreased until having a
26 second peak (about 0.8 ppb) around 20 p.m. The low concentration of SO_2 at night is likely due
27 to its deposition on the ground in the nocturnal boundary layer, while the increase in the
28 morning is induced by the mixing of the boundary layer allowing the entrainment of SO_2 from
29 aloft. On the non-event day, SO_2 concentration was throughout the day clearly lower than
30 typically on event days. The increase in the concentration occurred later than on event days
31 (around 10 a.m.), and the concentration reached only about 0.6 ppb. The second peak in the
32 evening was also clearly lower (about 0.3 ppb) than on event days. The diurnal cycle of sulfuric

1 acid proxy on NPF event days resembles the diurnal cycle of radiation; the concentration starts
2 to increase around 4 a.m. in the morning and is highest (median value $2.3 \times 10^7 \text{ cm}^{-3}$) around
3 noon. On the non-event day, sulfuric acid proxy stays lower than on event days, its maximum
4 value being about $1.7 \times 10^7 \text{ cm}^{-3}$. In addition, the value of the proxy starts to increase later than
5 on event days, reflecting the late increase in SO_2 concentration. These results are in agreement
6 with Hamed et al. (2006), who observed that in San Pietro Capofiume daytime SO_2
7 concentrations are clearly higher on NPF event days than on non-event days.

8 **3.2 Concentrations of sub-3nm clusters**

9 A high number of sub-3nm clusters was observed in San Pietro Capofiume during the
10 measurement period (Fig. 3). The total concentration of 1.5–1.8 nm clusters varied from 610 to
11 $11\,930 \text{ cm}^{-3}$ (5% and 95% percentile) with the median concentration of 2140 cm^{-3} . The total
12 concentration of 1.8–3.0 nm clusters varied from 2300 to $30\,150 \text{ cm}^{-3}$ (5% and 95% percentile),
13 while the median concentration was 7980 cm^{-3} . The majority of the observed sub-3nm clusters
14 were electrically neutral. The median concentrations of neutral clusters were 2090 cm^{-3} and
15 7950 cm^{-3} in the size bins of 1.5–1.8 nm and 1.8–3 nm, respectively. The median positive ion
16 concentrations were 20 cm^{-3} and 4 cm^{-3} in the same size bins, and the median negative ion
17 concentration was 6 cm^{-3} in both of the size bins. The concentrations of recombination products
18 were also low: the median concentrations were 11 cm^{-3} and 5 cm^{-3} in the size bins of 1.5–1.8
19 nm and 1.8–3 nm. The observed lower concentration of negative 1.5–1.8 nm ions compared to
20 positive ions is mainly caused by the lower sensitivity of the negative polarity of NAIS to detect
21 these ions, which results from slightly higher electrometer noise levels in corresponding
22 channels. On the other hand, the lower negative ion concentration can also be partly related to
23 the electrode effect, causing the accumulation of positive ions close to the Earth's surface
24 (Hoppel et al., 1967).

25 Our results are in agreement with the earlier measurements from boreal forest in Finland, where
26 a continuous population of sub-3nm neutral clusters has been observed (Lehtipalo et al., 2009;
27 Kulmala et al., 2013). However, the clusters concentrations observed in San Pietro Capofiume
28 are about five times higher than the concentrations in the same size range in boreal forest. The
29 observed cluster concentrations also exceed the concentrations of sub-3nm clusters reported
30 from a high-altitude site in France (Rose et al., 2015) and from two urban sites in the United
31 States (Yu et al., 2014). On the other hand, at polluted sites in China, the sub-3nm cluster
32 concentrations were observed to be of the same order of magnitude as in San Pietro Capofiume

1 (Xiao et al., 2015; Yu et al., 2015). This indicates that the formation of sub-3nm clusters may
2 be favored in areas where anthropogenic emissions of precursor vapors are high. Furthermore,
3 our results support the earlier observations from boreal forest, where the contribution of ion-
4 ion recombination to atmospheric cluster formation has been shown to be minor (Lehtipalo et
5 al., 2009; Kontkanen et al., 2013).

7 **3.3 New particle formation**

8 NPF events were frequently observed during the measurement campaign (see Fig. 4). During
9 the measurement period 86% (19/22) of the days, from which we had NAIS data, were
10 classified as NPF event days, while only one day was classified as a clear non-event case. On
11 average, NPF is detected at the site less frequently, on 40–45 % of the days in June and on 65–
12 70% of days in July (Hamed et al., 2007; Manninen et al., 2010). High frequency of NPF events
13 during our measurement campaign was likely related to favorable meteorological conditions
14 with high solar radiation and low RH (see Sect. 3.1). Figure 5 shows the evolution of ion size
15 distribution on a typical NPF event day (28 June) during the measurement campaign. The onset
16 of NPF event can be observed around 7 a.m. and the growth of the ions can be followed until 5
17 p.m. in the evening.

18 The statistics of particle growth rates for the NPF events are shown in Table 1. The median
19 growth rates in the size ranges of 1.5–3 nm, 3–7 nm and 7–20 nm were 4.3 nm h⁻¹, 6.0 nm h⁻¹
20 and 7.2 nm h⁻¹. Thus, the growth rate generally increased with the increasing particle size, which
21 has been observed also at other measurement sites (Yli-Juuti et al., 2011; Kuang et al., 2012;
22 Kulmala et al., 2013), and predicted by the so-called nano-Köhler theory describing the
23 activation of nanometer-sized clusters by organic vapors (Kulmala et al., 2004b). By using
24 BSMA (Balanced Scanning Mobility Analyzer) measurements, Manninen et al. (2010)
25 obtained the median growth rate of 1.5 nm h⁻¹ for 1.5–3 nm particles in San Pietro Capofiume.
26 The lower value of median growth rate compared to our results is likely caused by the fact that
27 the most of the events for which Manninen et al. (2010) were able to determine the sub-3nm
28 growth rate occurred in spring, when the production of condensable vapors is typically lower
29 than in summertime.

30 Table 2 presents the statistics of particle formation rates at 1.6 nm and at 2 nm during NPF
31 events. The median formation rate of 1.6 nm clusters, 45 cm⁻³ s⁻¹, was one order of magnitude
32 higher than the median formation rate of 2 nm clusters, 6.8 cm⁻³ s⁻¹. In earlier field

1 measurements in boreal forest, Finland, the median particle formation rates were $5.9 \text{ cm}^{-3} \text{ s}^{-1}$ at
2 1.5 nm and $1.9 \text{ cm}^{-3} \text{ s}^{-1}$ at 2 nm (Kulmala et al., 2013). On the other hand, at a polluted site in
3 Shanghai, China, the average formation rate of 1.3 nm clusters was observed to be $188 \text{ cm}^{-3} \text{ s}^{-1}$
4 (Xiao et al., 2015). Thus, it seems that the formation rates of sub-3nm clusters are in San
5 Pietro Capofiume higher than in clean boreal forest environment but still lower than at a
6 polluted urban site. This indicates that high background aerosol concentrations do not
7 necessarily inhibit the formation of sub-3nm clusters if the concentrations of precursor vapors
8 are high enough. The median condensation sink in San Pietro Capofiume was $1.1 \times 10^{-2} \text{ s}^{-1}$ during
9 the measurement period. In boreal forest, Finland, typical condensation sink on NPF event days
10 has been observed to be about $2 \times 10^{-3} \text{ s}^{-1}$ (Dal Maso et al., 2005; Kulmala et al., 2013), and in
11 Shanghai, China, $6 \times 10^{-2} \text{ s}^{-1}$ (Xiao et al., 2015).

12 The median formation rates of 1.6 nm positive and negative ions ($0.19 \text{ cm}^{-3} \text{ s}^{-1}$ and $0.06 \text{ cm}^{-3} \text{ s}^{-1}$)
13 were two orders of magnitude lower than the formation rate of 1.6 nm total clusters (Table
14 2). In addition, the median formation rates of 2 nm positive ions ($0.12 \text{ cm}^{-3} \text{ s}^{-1}$) and negative
15 ions ($0.08 \text{ cm}^{-3} \text{ s}^{-1}$) were one order of magnitude lower than the formation rate of 2 nm total
16 clusters. Thus, neutral pathways seem to dominate particle formation in San Pietro Capofiume.
17 These results are consistent with the earlier observations from boreal forest in Finland and at a
18 high-altitude site in France, where the formation rate of 1.5 nm total clusters has been found to
19 clearly exceed the formation rate of 1.5 nm ions (Kulmala et al., 2013; Rose et al., 2015).
20 Manninen et al. (2010) reported slightly lower values for the median formation rates of 2 nm
21 ions ($0.06 \text{ cm}^{-3} \text{ s}^{-1}$ for both polarities) based on their BSMA measurements in San Pietro
22 Capofiume. Note that the lower formation rate of 1.6 nm negative ions than positive ions in our
23 measurements is mainly due to the lowered sensitivity of negative polarity of the NAIS to detect
24 1.5–1.8 nm ions.

25 To further investigate the contribution of ions to particle formation, we calculated the ion-
26 induced nucleation fraction for each NPF event by dividing the ion formation rate by the total
27 formation rate. The median ion-induced nucleation fraction was 0.7% at 1.6 nm and 3.0% at 2
28 nm. When the contribution of ion-ion recombination is also taken into account, the total ion-
29 mediated nucleation fraction becomes 0.8% at 1.6 nm and 3.7% at 2 nm. This further
30 demonstrates that ions have only a minor contribution to the formation of sub-3nm clusters in
31 San Pietro Capofiume. The higher ion-induced nucleation fraction at 2 nm than at 1.6 nm
32 suggests that ions at 2 nm may be formed by coagulation between small ions and neutral

1 clusters. In previous studies the ion-induced nucleation fraction has been observed to be
2 typically low, less than 10%, in the continental boundary layer (Iida et al., 2006; Manninen et
3 al., 2010).

4

5 **3.4 Diurnal variation of cluster concentrations and formation rates**

6 Figure 6 shows the median diurnal variation of the concentrations of neutral clusters, charged
7 clusters and recombination products on NPF event days and on the only non-event day. In
8 addition, the variation of PBL height is presented. The concentrations of neutral 1.5–1.8 nm
9 and 1.8–3.0 nm clusters were high throughout the day on NPF event days and on the non-event
10 day. On NPF event days the neutral cluster concentrations had maxima around 9 a.m., which
11 could not be observed on the non-event day. The concentration maximum occurred slightly
12 earlier in the size bin of 1.5–1.8 nm than in the larger, 1.8–3 nm, size bin. The daytime
13 maximum on NPF event days can also be detected in the concentrations of ions and
14 recombination product in the size bin of 1.8–3.0 nm. Nevertheless, the peak ion concentrations
15 were about three orders of magnitude lower than those of neutral clusters. In the smaller size
16 bin (1.5–1.8 nm) these maxima were not as clear. The reason for this is that small ions are
17 continuously formed in the atmosphere as a result of ionization of air molecules, while larger
18 ions are usually present only during NPF events (e.g. Hirsikko et al., 2011). The observed
19 diurnal cycle of the cluster concentrations is generally similar as in the earlier observations
20 made in boreal forest, Finland (Kulmala et al., 2013), and at urban sites in the United States and
21 China (Yu et al., 2014; Xiao et al., 2015; Yu et al., 2015).

22 To study the contribution of ions to cluster concentrations, we also examined the median diurnal
23 variation of the fraction of ions of all clusters on NPF event days (Fig. 7). The ion fraction in
24 the size bin of 1.5–1.8 nm varied between 0.3% and 2%. The lowest values were obtained
25 slightly after 9 a.m., which is due to the strong increase in the neutral cluster concentration
26 during NPF event (Fig. 6). In the size bin of 1.8–3 nm, the ion fraction was most of the time
27 very low (about 0.2%), but peaked before 9 a.m. reaching 0.5%. This is caused by the fact that
28 the concentration of ions in the size bin of 1.8–3 nm started to increase earlier on NPF event
29 days than the concentration of neutral clusters in the same size bin (Fig. 6). The earlier
30 formation of charged than neutral clusters has previously been observed at several European
31 measurement sites (Manninen et al., 2010; Gonser et al., 2014). One possible explanation for
32 this is the enhancement of activation of clusters in the presence of charge (e.g. Yu and Turco,

1 2000; Winkler et al., 2008), which allows charged clusters to activate earlier than neutral
2 clusters when the concentration of low-volatile vapors increases in the morning. This may
3 indicate that ion-mediated nucleation pathways could be more significant in the conditions with
4 low precursors vapor concentrations.

5 In Fig. 8 the median diurnal variations of particle formation rates are presented together with
6 the PBL height for NPF event days and for the only non-event day. The formation rate of 1.6
7 nm total clusters varied between 8 and 68 $\text{cm}^{-3} \text{s}^{-1}$ on NPF event days, reaching the highest
8 values around 9 a.m. On the non-event day the formation rate was lower, varying between 2
9 and 14 $\text{cm}^{-3} \text{s}^{-1}$. Similarly, the formation rate of 2 nm clusters had a maximum of 7 $\text{cm}^{-3} \text{s}^{-1}$ on
10 NPF event days, and on the non-event day it varied between 0.1 and 3 $\text{cm}^{-3} \text{s}^{-1}$. The formation
11 rates of ions were at both sizes clearly lower than the total formation rates. The maximum
12 formation rate of 1.6 nm ions on NPF event days was 0.19 $\text{cm}^{-3} \text{s}^{-1}$ for positive ions and 0.09
13 $\text{cm}^{-3} \text{s}^{-1}$ for negative ions. At 2 nm, the corresponding maximum formation rate was 0.13 cm^{-3}
14 s^{-1} for positive ions and 0.11 $\text{cm}^{-3} \text{s}^{-1}$ for negative ions. On the non-event day the ion formation
15 rates were even lower than on event days. Overall, these results suggest that sub-3nm clusters
16 are formed continuously, also outside NPF events. Furthermore, as concluded already above,
17 neutral nucleation mechanisms seem to dominate in San Pietro Capofiume. Our results support
18 earlier observations obtained in field measurement in boreal forest by Kulmala et al. (2013).

19 When comparing the diurnal variations of cluster concentrations and their formation rates with
20 the diurnal cycle of PBL height and other meteorological parameters, similarities can be found.
21 At the same time as the concentrations and formation rates of clusters started to increase in the
22 morning of NPF event days, after 7 a.m., the PBL height also started to increase. Furthermore,
23 at this time radiation, temperature and SO_2 concentration had already started to rise from their
24 low night-time values and, reversely, RH and condensation sink were decreasing (Fig. 2). This
25 indicates that the sunrise can be important for the formation of atmospheric clusters due to
26 several processes. Firstly, the build-up of PBL, induced by the heating of solar radiation, dilutes
27 the background aerosol concentration and thus reduces the condensation sink. Furthermore, the
28 mixing of the boundary layer increases the concentration of SO_2 , which is oxidized to sulfuric
29 acid. Solar radiation also triggers the photochemical production of other low-volatile precursor
30 vapors, which could participate in the formation of clusters. Finally, increasing temperature
31 also lowers RH. On the other hand, it needs to be noted that the formation of sub-2nm clusters
32 was observed to take place continuously, also at night (see Fig. 8). Thus, the formation of the

1 smallest clusters seems to occur also without solar radiation, which indicates that they may be
2 formed, for example, by the low-volatile vapors produced in the ozonolysis of organic vapors
3 (Ehn et al., 2014; Jokinen et al., 2014).

4

5 **3.5 Effect of sulfuric acid concentration and condensation sink on cluster** 6 **concentrations**

7 San Pietro Capofiume is located in the industrialized Po Valley with many emission sources for
8 anthropogenic pollutants. According to Sogacheva et al. (2007), more than 40% of SO₂
9 emissions over the Po Valley can be observed at the San Pietro Capofiume station. SO₂ is a
10 precursor for sulfuric acid that is known to be a key compound in atmospheric cluster formation
11 (e.g. Weber et al., 1997; Sipilä et al., 2010; Kirkby et al., 2011). To investigate the importance
12 of sulfuric acid for cluster formation in San Pietro Capofiume, we studied the correlation
13 between the concentrations of neutral and charged clusters and sulfuric acid proxy.
14 Furthermore, to see how the concentrations of large background aerosol particles affect cluster
15 concentrations, the correlation between cluster concentrations and condensation sink was
16 examined.

17 In agreement with earlier studies, the sub-3nm cluster concentrations correlated positively with
18 sulfuric acid proxy indicating that sulfuric acid possibly participates in the cluster formation in
19 San Pietro Capofiume (Fig. 9). For both neutral and charged clusters the positive correlation
20 was stronger in the size bin of 1.8–3 nm ($R = 0.64$ for neutral clusters and $R = 0.67$ for ions)
21 than in the size bin of 1.5–1.8 nm ($R = 0.52$ for neutral clusters and $R = 0.51$ for ions). This is
22 in accordance with Kulmala et al. (2013), who observed that the smallest, sub-1.7 nm, clusters
23 correlated with sulfuric acid less strongly than larger clusters.

24 The relation between the sub-3nm cluster concentrations and condensation sink is presented in
25 Fig. 10. It seems that the concentration of neutral clusters does not have a negative correlation
26 with condensation sink as one would expect. This indicates that in San Pietro Capofiume the
27 formation of neutral clusters may, at least partly, be linked to anthropogenic emissions with
28 high concentrations of low-volatile precursor vapors but also high condensation sink.
29 Furthermore, ions had a negative correlation with the condensation sink especially in the size
30 bin of 1.5–1.8 nm ($R = -0.56$). In the size bin of 1.8–3 nm the negative correlation was weaker
31 ($R = -0.33$). We also investigated the correlation between the cluster concentrations and the
32 ratio of sulfuric acid proxy to condensation sink. The correlation coefficients obtained between

1 this ratio and the neutral cluster concentrations were slightly lower than between neutral clusters
2 and only sulfuric acid ($R = 0.51$ in the size bin of 1.5–1.8 nm and $R = 0.62$ in the size bin of
3 1.8–3 nm). On the other hand, for ions the correlation coefficients were slightly higher in this
4 case ($R = 0.57$ in the size bin of 1.5–1.8 nm and $R = 0.69$ in the size bin of 1.8–3 nm).

5

6 **3.6 Effect of air mass origin**

7 By using back-trajectory analysis, we investigated how the air mass origin affects the sub-3nm
8 cluster concentrations, and their precursors and sinks in San Pietro Capofiume. Figure 11
9 illustrates the air mass arrival directions and their relation to the total concentration of 1.8–3.0
10 nm clusters, sulfuric acid proxy, and condensation sink in San Pietro Capofiume around midday
11 (between 10 a.m. and 2 p.m.). A clear majority of air masses arrived to San Pietro Capofiume
12 from northeastern to eastern directions and from the southwest during the measurement
13 campaign. When air masses were coming from northeastern to eastern directions the sub-3nm
14 cluster concentrations were most of the time high ($>3 \times 10^4 \text{ cm}^{-3}$). When air masses originated
15 from the southwest, lower concentrations were more frequent. Moreover, the southwestern
16 direction was often related to high condensation sink ($>1.2 \times 10^{-2} \text{ s}^{-1}$). On the other hand, high
17 values of condensation sink were observed also when air masses were coming from the
18 northeast. For sulfuric acid proxy, there was no clear difference between the northeastern and
19 southwestern directions, but high concentrations ($>2.4 \times 10^7 \text{ cm}^{-3}$) were linked to both of these
20 directions.

21 All in all, it seems that the northeastern direction was more favorable for the formation of sub-
22 3nm clusters than the southwestern direction during our measurement campaign. In previous
23 studies air masses related to particle formation have also been observed to arrive to San Pietro
24 Capofiume mostly from eastern directions (Hamed et al., 2007; Sogacheva et al., 2007).
25 Furthermore, Hamed et al. (2007) reported that in all seasons except summer, the eastern
26 directions were associated with the lower value of condensation sink than the western
27 directions. In summer, they did not observe a clear difference in condensation sink between
28 eastern and western air masses. This is in agreement with our results which do not show
29 significantly lower condensation sink related to the northwestern direction than the
30 southwestern direction. Thus, it seems that during our measurement campaign the precursor
31 vapors of the clusters and large background aerosol particles, which act as a sink for clusters,
32 may have originated from the same sources. This is consistent with the fact that no negative

1 correlation was found between neutral sub-3nm clusters and condensation sink, as discussed in
2 Sect. 3.5. The possible sources of background aerosol particles and precursor vapors include
3 anthropogenic emissions from power plants and industrial areas in the Po Valley, ship traffic in
4 the Adriatic Sea, and long-range transport from Central and Eastern Europe (see Fig. 1) (Hamed
5 et al., 2007; Sogacheva et al., 2007).

6

7 **4 Conclusions**

8 A high concentration of sub-3nm clusters was observed in San Pietro Capofiume measurement
9 site during the PEGASOS campaign (7 June – 9 July 2012). The majority of clusters were
10 electrically neutral. The observed sub-3nm cluster concentrations were of the same order of
11 magnitude as at polluted sites in China (Xiao et al. 2015; Yu et al., 2015), and higher than in
12 clean boreal forest in Finland (Kulmala et al., 2013) and at urban sites in the United States (Yu
13 et al., 2014).

14 New particle formation (NPF) events were observed during the measurement period very
15 frequently, on 86% of the days. The particle formation rates during events were higher than in
16 clean boreal forest environment but lower than at a highly polluted urban site (Kulmala et al.,
17 2013; Xiao et al., 2015). Furthermore, the median formation rates of ions were clearly lower
18 than the formation rates of total clusters at all sizes. This indicates that neutral pathways
19 dominate the sub-3nm cluster formation in San Pietro Capofiume, similarly as in boreal forest
20 (Kulmala et al., 2013). The median condensation sink during the measurement period was
21 relatively high, which demonstrates that high background aerosol concentrations do not
22 necessarily inhibit the formation of sub-3nm clusters.

23 The neutral cluster concentrations were found to have maxima in the mornings of NPF event
24 days, which were absent on the non-event day. Still, the formation of the smallest clusters was
25 observed to take place continuously, also outside NPF events. The increase in the cluster
26 concentration in the morning took place simultaneously with the build-up of planetary boundary
27 layer (PBL). In addition, radiation, temperature and SO₂ concentration were rising and
28 condensation sink and RH declining at that time. Thus, the changes in the local meteorological
29 conditions triggered by the sunrise in the morning may be important drivers of cluster formation
30 at the San Pietro Capofiume station.

31 The sub-3nm cluster concentrations were observed to have a positive correlation with sulfuric
32 acid proxy. This suggests that sulfuric acid may have an important role in the formation of sub-

1 3nm clusters in San Pietro Capofiume, as has also been observed at other measurement sites
2 (Kulmala et al., 2013; Yu et al., 2014). On the other hand, it is likely that other compounds, e.g.
3 low-volatile organic vapors, also participate in the formation of clusters. The concentration of
4 charged clusters was found to have a negative correlation with condensation sink, while no
5 relation between the neutral cluster concentrations and condensation sink was observed. This
6 result, together with the back-trajectory analysis, indicates that the precursor vapors of clusters
7 and background aerosol particles, acting as their sink, may have originated from the same
8 sources. The potential sources include anthropogenic emissions from power plants and
9 industrial areas in the Po Valley, maritime traffic in the Adriatic Sea, and long-range transport
10 from Central and Eastern Europe (Hamed et al., 2007; Sogacheva et al., 2007).

11

12 **Acknowledgements**

13 This research was supported by the European Commission under the Framework Programme 7
14 (PEGASOS project, FP7-ENV-2010-265148), the European Research Council (ERC)
15 Advanced Grant (ATM-NUCLE, 227463), and the European Union's Horizon 2020 research
16 and innovation programme under the Marie Skłodowska-Curie grant agreement No. 656994.
17 The support by the Academy of Finland Centre of Excellence program (project no. 1118615
18 and 272041) is also gratefully acknowledged.

19

1 **References**

- 2 Aalto, P., Hämeri, K., Becker, E., Weber, R., Salm, J., Mäkelä, J.M., Hoell, C., O'Dowd, C.D.,
3 Karlsson, H., Hansson, H.-C., Väkevää M., Koponen, I.K., Buzorius, G. and Kulmala, M.:
4 Physical characterization of aerosol particles during nucleation events, *Tellus*, 53 B, 344–358,
5 2001.
- 6 Almeida, J., Schobesberger, S., Kurten, A., Ortega, I., Kupiainen-Määttä, O., Praplan, A.,
7 Adamov, A., Amorim, A., Bianchi, F., Breitenlechner, M., David, A., Dommen, J., Donahue,
8 N., Downard, A., Dunne, E., Duplissy, J., Ehrhart, S., Flagan, R., Franchin, A., Guida, R.,
9 Hakala, J., Hansel, A., Heinritzi, M., Henschel, H., Jokinen, T., Junninen, H., Kajos, M.,
10 Kangasluoma, J., Keskinen, H., Kupc, A., Kurten, T., Kvashin, A., Laaksonen, A., Lehtipalo,
11 K., Leiminger, M., Leppä, J., Loukonen, V., Makhmutov, V., Mathot, S., McGrath, M.,
12 Nieminen, T., Olenius, T., Onnela, A., Petaja, T., Riccobono, F., Riipinen, I., Rissanen, M.,
13 Rondo, L., Ruuskanen, T., Santos, F., Sarnela, N., Schallhart, S., Schnitzhofer, R., Seinfeld, J.,
14 Simon, M., Sipila, M., Stozhkov, Y., Stratmann, F., Tome, A., Trostl, J., Tsagkogeorgas, G.,
15 Vaattovaara, P., Viisanen, Y., Virtanen, A., Vrtala, A., Wagner, P., Weingartner, E., Wex, H.,
16 Williamson, C., Wimmer, D., Ye, P., Yli-Juuti, T., Carslaw, K., Kulmala, M., Curtius, J.,
17 Baltensperger, U., Worsnop, D., Vehkamäki, H., and Kirkby, J.: Molecular understanding of
18 sulphuric acid-amine particle nucleation in the atmosphere, *Nature*, 502, 359–363,
19 doi:10.1038/nature12663, 2013.
- 20 Angelini, A., and Gobbi, G. P.: Some remarks about lidar data preprocessing and different
21 implementations of the gradient method for determining the aerosol layers, *Annals Geophys*,
22 57, 2, 515 2014, A0218; doi:10.4401/ag-6408, 2014.
- 23 Boy, M. and Kulmala, M.: Nucleation events in the continental boundary layer: Influence of
24 physical and meteorological parameters, *Atmos. Chem. Phys.*, 2, 1–16, doi:10.5194/acp-2-1-
25 2002, 2002.
- 26 Dal Maso, M., Kulmala, M., Riipinen, I., Wagner, R., Hussein, T., Aalto, P. P., and Lehtinen,
27 K. E. J.: Formation and growth of fresh atmospheric aerosols: Eight years of aerosol size
28 distribution data from SMEAR II, Hyytiälä, Finland, *Boreal Environ. Res.*, 10, 323–336, 2005.
- 29 Di Giuseppe, F., A. Riccio, L. Caporaso, G. Bonafè, G. P. Gobbi, F. Angelini, Automatic
30 detection of atmospheric boundary layer height using ceilometer backscatter data assisted by a

1 boundary layer model, *Quarterly Journal of the Royal Meteorological Society*, 138, 649–663,
2 doi:10.1002/qj.964, 2012.

3 Draxler, R. R. and Rolph, G. D.: HYSPLIT (HYbrid Single-Particle Lagrangian Integrated
4 Trajectory), model access via NOAA ARL READY Website, NOAA Air Resources
5 Laboratory, Silver Spring, MD, available at: <http://www.arl.noaa.gov/ready/hysplit4.html> (last
6 access: 13.1.2015).

7 Ehn, M., Thornton, J. A., Kleist, E., Sipilä, M., Junninen, H., Pullinen, I., Springer, M., Rubach,
8 F., Tillmann, R., Lee, B., Lopez-Hilfiker, F., Andres, S., Acir, I.-H., Rissanen, M., Jokinen, T.,
9 Schobesberger, S., Kangasluoma, J., Kontkanen, J., Nieminen, T., Kurtén, T., Nielsen, L. B.,
10 Jørgensen, S., Kjaergaard, H. G., Canagaratna, M., Dal Maso, M., Berndt, T., Petäjä, T.,
11 Wahner, A., Kerminen, V., Kulmala, M., Worsnop, D. R., Wildt, J, and Mentel, T. F.: A large
12 source of low-volatility secondary organic aerosol, *Nature*, 506, 476–479,
13 doi:10.1038/nature13032, 2014.

14 Gonser, S. G., Klein, F., Birmili, W., Größ, J., Kulmala, M., Manninen, H. E.,
15 Wiedensohler, A., and Held, A.: Ion – particle interactions during particle formation and
16 growth at a coniferous forest site in central Europe, *Atmos. Chem. Phys.*, 14, 10547–10563,
17 doi:10.5194/acp-14-10547-2014, 2014.

18 Günther, A. B., Jiang, X., Heald, C. L., Sakulyanontvittaya, T., Duhl, T., Emmons, L. K.,
19 and Wang, X.: The Model of Emissions of Gases and Aerosols from Nature version 2.1
20 (MEGAN2.1): an extended and updated framework for modeling biogenic emissions, *Geosci.*
21 *Model Dev.*, 5, 1471–1492, doi:10.5194/gmd-5-1471-2012, 2012.

22 Hamed, A., Joutsensaari, J., Mikkonen, S., Sogacheva, L., Dal Maso, M., Kulmala, M., Cavalli,
23 F., Fuzzi, S., Facchini, M.C., Decesari, S., Mircea, M., Lehtinen, K.E.J., Laaksonen, A.:
24 Nucleation and growth of new particles in Po Valley, Italy. *Atmos. Chem. Phys.* 7, 355–376,
25 2007.

26 Hamed, A., Korhonen, H., Sihto, S.-L., Joutsensaari, J., Järvinen, H., Petäjä, T., Arnold, F.,
27 Nieminen, T., Kulmala, M., Smith, J. N., Lehtinen, K. E. J., and Laaksonen, A.: The role of
28 relative humidity in continental new particle formation, *J. Geophys. Res.*, 116, D03202,
29 doi:10.1029/2010JD014186, 2011.

1 Hirsikko, A., Laakso, L., Hörrak, U., Aalto, P. P., Kerminen, V.-M., and Kulmala, M.: Annual
2 and size dependent variation of growth rates and ion concentrations in boreal forest, *Boreal*
3 *Environ. Res.*, 10, 357–369, 2005.

4 Hirsikko, A., Bergman, T., Laakso, L., Dal Maso, M., Riipinen, I., Hörrak, U., and
5 Kulmala, M.: Identification and classification of the formation of intermediate ions measured
6 in boreal forest, *Atmos. Chem. Phys.*, 7, 201–210, doi:10.5194/acp-7-201-2007, 2007.

7 Hirsikko, A., Nieminen, T., Gagné, S., Lehtipalo, K., Manninen, H. E., Ehn, M., Hörrak, U.,
8 Kerminen, V.-M., Laakso, L., McMurry, P. H., Mirme, A., Mirme, S., Petäjä, T., Tammet, H.,
9 Vakkari, V., Vana, M., and Kulmala, M.: Atmospheric ions and nucleation: a review of
10 observations, *Atmos. Chem. Phys.*, 11, 767–798, doi:10.5194/acp-11-767-2011, 2011.

11 Hoppel, W. A.: Theory of the electrode effect, *Journal of Atmospheric and Terrestrial Physics*,
12 29, 709–721, 1967.

13 Hyvönen, S., Junninen, H., Laakso, L., Dal Maso, M., Grönholm, T., Bonn, B., Keronen, P.,
14 Aalto, P., Hiltunen, V., Pohja, T., Launiainen, S., Hari, P., Mannila, H., and Kulmala, M.: A
15 look at aerosol formation using data mining techniques, *Atmos. Chem. Phys.*, 5, 3345–3356,
16 doi:10.5194/acp-5-3345-2005, 2005.

17 Iida, K., Stolzenburg, M., McMurry, P. H., Dunn, M. J., Smith, J. N., Eisele, F., and Keady, P.:
18 Contribution of ion-induced nucleation to new particle formation: Methodology and its
19 application to atmospheric observations in Boulder, Colorado, *J. Geophys. Res.*, 111, D23201,
20 doi:10.1029/2006JD007167, 2006.

21 Jokinen, T., Sipilä, M., Richters, S., Kerminen, V.-M., Paasonen, P., Stratmann, F., Worsnop,
22 D., Kulmala, M., Ehn, M., Herrmann, H., and Berndt, T.: Rapid Autoxidation Forms Highly
23 Oxidized RO₂ Radicals in the Atmosphere, *Angew. Chem. Internat. Ed.*, 53, 14596–14600,
24 doi:10.1002/anie.201408566, 2014.

25 Kangasluoma, J., Junninen, H., Lehtipalo, K., Sipilä, M., Mikkilä, J., Vanhanen, J., Attoui,
26 M., Worsnop, D., Kulmala, M., and Petäjä, T.: Remarks on ion generation for CPC calibrations
27 in the sub 3 nm size range, *Aerosol Sci. Tech.*, 47, 556–563,
28 doi:10.1080/02786826.2013.773393, 2013.

29 Kazil, J., Stier, P., Zhang, K., Quaas, J., Kinne, S., O'Donnell, D., Rast, S., Esch, M., Ferrachat,
30 S., Lohmann, U., and Feichter, J.: Aerosol nucleation and its role for clouds and Earth's

1 radiative forcing in the aerosol-climate model ECHAM5-HAM, *Atmos. Chem. Phys.*, 10,
2 10733–10752, doi:10.5194/acp-10-10733-2010, 2010.

3 Kerminen, V.-M., Pirjola, L., and Kulmala, M.: How significantly does coagulation
4 scavenging limit atmospheric particle production?, *J. Geophys. Res.*, 125, 24, 119–24, 125,
5 2001.

6 Kirkby, J., Curtius, J., Almeida, J., Dunne, E., Duplissy, J., Ehrhart, S., Franchin, A., Gagné,
7 S., Ickes, L., Kürten, A., Kupc, A., Metzger, A., Riccobono, F., Rondo, L., Schobesberger, S.,
8 Tsagkogeorgas, G., Wimmer, D., Amorim, A., Bianchi, F., Breitenlechner, M., David, A.,
9 Dommen, J., Downard, A., Ehn, M., Flagan, R. C., Haider, S., Hansel, A., Hauser, D., Jud, W.,
10 Junninen, H., Kreissl, F., Kvashin, A., Laaksonen, A., Lehtipalo, K., Lima, J., Lovejoy, E. R.,
11 Makhutov, V., Mathot, S., Mikkilä, J., Minginette, P., Mogo, S., Nieminen, T., Onnela, A.,
12 Pereira, A., Petäjä, T., Schnitzhofer, R., Seinfeld, J. H., Sipilä, M., Stozhkov, Y., Stratmann, F.,
13 Tome, A., Vanhanen, J., Viisanen, Y., Virtala, A., Wagner, P. E., Walther, H., Weingartner, E.,
14 Wex, H., Winkler, P. M., Carslaw, K. S., Worsnop, D. R., Baltensperger, U., and Kulmala, M.:
15 The role of sulfuric acid, ammonia and galactic cosmic rays in atmospheric aerosol nucleation,
16 *Nature*, 476, 429–433, 2011.

17 Kontkanen, J., Lehtinen, K. E. J., Nieminen, T., Manninen, H. E., Lehtipalo, K., Kerminen, V.-
18 M., and Kulmala, M.: Estimating the contribution of ion–ion recombination to sub-2 nm cluster
19 concentrations from atmospheric measurements, *Atmos. Chem. Phys.*, 13, 11391–11401,
20 doi:10.5194/acp-13-11391-2013, 2013.

21 Korhonen, H., Sihto, S.-L., Kerminen, V.-M., and Lehtinen, K. E. J.: Evaluation of the
22 accuracy of analysis tools for atmospheric new particle formation, *Atmos. Chem. Phys.*, 11,
23 3051–3066, doi:10.5194/acp-11-3051-2011, 2011.

24 Kuang, C., Chen, M., Zhao, J., Smith, J., McMurry, P. H., and Wang, J.: Size and time-resolved
25 growth rate measurements of 1 to 5 nm freshly formed atmospheric nuclei, *Atmos. Chem.*
26 *Phys.*, 12, 3573–3589, doi:10.5194/acp-12-3573-2012, 2012.

27 Kulmala, M., Toivonen, A., Mäkelä, J. M., and Laaksonen, A.: Analysis of the growth of
28 nucleation mode particles observed in Boreal forest, *Tellus*, 50B, 449–462, 1998.

29 Kulmala, M., Maso, M. D., Mäkelä, J. M., Pirjola, L., Väkevä, M., Aalto, P., Miikkulainen, P.,
30 Hämeri, K. and O'Dowd, C. D.: On the formation, growth and composition of nucleation mode
31 particles. *Tellus B*, 53: 479–490, 2001.

1 Kulmala, M., Vehkamäki, H., Petäjä, T., Dal Maso, M., Lauri, A., Kerminen, V.-M., Birmili,
2 W., and McMurry P. H. Formation and growth rates of ultrafine atmospheric particles: A review
3 of observations, *J. Aerosol Sci.*, 35, 143–176, 2004a.

4 Kulmala, M., Kerminen, V.-M., Anttila, T., Laaksonen, A., and O’Dowd, C. D.: Organic
5 aerosol formation via sulphate cluster activation, *J. Geophys. Res.*, 109(D4), 4205,
6 doi:10.1029/2003JD003961, 2004b.

7 Kulmala, M., Riipinen, I., Sipilä, M., Manninen, H.E., Petaja, T., Junninen, H., dal Maso, M.,
8 Mordas, G., Mirme, A., Vana, M., Hirsikko, A., Laasko, L., Harrison, R.M., Hanson, I., Leung,
9 C., Lehtinen, K.E.J., Kerminen, V.-M., Toward direct measurement of atmospheric nucleation.
10 *Science* 318 (5847), 89–92, 2007.

11 Kulmala, M., Petäjä, T., Nieminen, T., Sipilä, M., Manninen, H. E., Lehtipalo, K., Dal Maso,
12 M., Aalto, P. P., Junninen, H., Paasonen, P., Riipinen, I., Lehtinen, K. E. J., Laaksonen, A., and
13 Kerminen, V.-M.: Measurement of the nucleation of atmospheric aerosol particles, *Nat. Protoc.*,
14 7, 1651–1667, doi:10.1038/nprot.2012.091, 2012.

15 Kulmala, M., Kontkanen, J., Junninen, H., Lehtipalo, K., Manninen, H. E., Nieminen, T.,
16 Petäjä, T., Sipilä, M., Schobesberger, S., Rantala, P., Franchin, A., Jokinen, T., Järvinen, E.,
17 Äijälä, M., Kangasluoma, J., Hakala, J., Aalto, P. P., Paasonen, P., Mikkilä, J., Vanhanen, J.,
18 Aalto, J., Hakola, H., Makkonen, U., Ruuskanen, T., Mauldin, R. L., Duplissy, J., Vehkamäki,
19 H., Bäck, J., Kortelainen, A., Riipinen, I., Kurtén, T., Johnston, M. V., Smith, J. N., Ehn, M.,
20 Mentel, T. F., Lehtinen, K. E. J., Laaksonen, A., Kerminen, V.-M., and Worsnop, D. R.: Direct
21 observations of atmospheric aerosol nucleation, *Science*, 339, 943–946,
22 doi:10.1126/science.1227385, 2013.

23 Kulmala, M., Petäjä, T., Ehn, M., Thornton, J., Sipilä, M., Worsnop, D. R., and Kerminen, V.-
24 M.: Chemistry of atmospheric nucleation: on the recent advances on precursor characterization
25 and atmospheric cluster composition in connection with atmospheric new particle formation,
26 *Annu. Rev. Phys. Chem.*, 65, 21–37, 2014.

27 Laakso, L., Petäjä, T., Lehtinen, K. E. J., Kulmala, M., Paatero, J., Hörrak, U., Tammet, H.,
28 and Joutsensaari, J.: Ion production rate in a boreal forest based on ion, particle and radiation
29 measurements, *Atmos. Chem. Phys.*, 4, 1933–1943, doi:10.5194/acp-4-1933-2004, 2004.

30 Laaksonen, A., Hamed, A., Joutsensaari, J., Hiltunen, L., Cavalli, F., Junkermann, W., Asmi,
31 A., Fuzzi, S., and Facchini, M. C.: Cloud condensation nucleus production from nucleation

1 events at a highly polluted region, *Geophys. Res. Lett.*, 32, L06812,
2 doi:10.1029/2004GL022092, 2005.

3 Lehtipalo, K., Sipilä, M., Riipinen, I., Nieminen, T., and Kulmala, M.: Analysis of atmospheric
4 neutral and charged molecular clusters in boreal forest using pulse-height CPC, *Atmos. Chem.*
5 *Phys.*, 9, 4177–4184, doi:10.5194/acp-9-4177-2009, 2009.

6 Lehtipalo, K., Kulmala, M., Sipilä, M., Petäjä, T., Vana, M., Ceburnis, D., Dupuy, R., and
7 O'Dowd, C.: Nanoparticles in boreal forest and coastal environment: a comparison of
8 observations and implications of the nucleation mechanism, *Atmos. Chem. Phys.*, 10, 7009–
9 7016, doi:10.5194/acp-10-7009-2010, 2010.

10 Makkonen, R., Asmi, A., Kerminen, V.-M., Boy, M., Arneth, A., Hari, P., and Kulmala, M.:
11 Air pollution control and decreasing new particle formation lead to strong climate warming,
12 *Atmos. Chem. Phys.*, 12, 1515–1524, doi:10.5194/acp-12-1515-2012, 2012.

13 Manninen, H. E., Nieminen, T., Asmi, E., Gagné, S., Häkkinen, S., Lehtipalo, K., Aalto, P.,
14 Vana, M., Mirme, A., Mirme, S., Hörrak, U., Plass-Dülmer, C., Stange, G., Kiss, G., Hoffer,
15 A., Törö, N., Moerman, M., Henzing, B., de Leeuw, G., Brinkenberg, M., Kouvarakis, G. N.,
16 Bougiatioti, A., Mihalopoulos, N., O'Dowd, C., Ceburnis, D., Arneth, A., Svenningsson, B.,
17 Swietlicki, E., Tarozzi, L., Decesari, S., Facchini, M. C., Birmili, W., Sonntag, A.,
18 Wiedensohler, A., Boulon, J., Sellegri, K., Laj, P., Gysel, M., Bukowiecki, N., Weingartner,
19 E., Wehrle, G., Laaksonen, A., Hamed, A., Joutsensaari, J., Petäjä, T., Kerminen, V.-M., and
20 Kulmala, M.: EUCAARI ion spectrometer measurements at 12 European sites - analysis of new
21 particle formation events, *Atmos. Chem. Phys.*, 10, 7907–7927, doi:10.5194/acp-10-7907-
22 2010, 2010.

23 Merikanto, J., Spracklen, D. V., Mann, G. W., Pickering, S. J., and Carslaw, K. S.: Impact of
24 nucleation on global CCN, *Atmos. Chem. Phys.*, 9, 8601–8616, doi:10.5194/acp-9-8601-2009,
25 2009.

26 Metzger, A., Verheggen, B., Dommen, J., Duplissy, J., Prevot, A. S., Weingartner, E., Riipinen,
27 I., Kulmala, M., Spracklen, D. V., Carslaw, K. S., and Baltensperger, U.: Evidence for the role
28 of organics in aerosol particle formation under atmospheric conditions, *P. Natl. Acad. Sci.*, 107,
29 6646–6651, doi:10.1073/pnas.0911330107, 2010.

30 Mikkonen, S., Romakkaniemi, S., Smith, J. N., Korhonen, H., Petäjä, T., Plass-Düelmer, C.,
31 Boy, M., McMurry, P. H., Lehtinen, K. E. J., Joutsensaari, J., Hamed, A., Mauldin III, R. L.,

1 Birmili, W., Spindler, G., Arnold, F., Kulmala, M., and Laaksonen, A.: A statistical proxy for
2 sulphuric acid concentration, *Atmos. Chem. Phys.*, 11, 11319–11334, doi:10.5194/acp-11-
3 11319-2011, 2011.

4 Mirme, S., Mirme, A., Minikin, A., Petzold, A., Hörrak, U., Kerminen, V.-M., and Kulmala,
5 M.: Atmospheric sub-3nm particles at high altitudes, *Atmos. Chem. Phys.*, 10, 437–451,
6 doi:10.5194/acp-10-437-2010, 2010.

7 Mirme, S. and Mirme, A.: The mathematical principles and design of the NAIS – a
8 spectrometer for the measurement of cluster ion and nanometer aerosol size distributions,
9 *Atmos. Meas. Tech.*, 6, 1061–1071, doi:10.5194/amt-6-1061-2013, 2013.

10 Nadykto, A. B., and Yu, F.: Uptake of neutral polar vapour molecules by charged
11 clusters/particles: Enhancement due to dipole-charge interaction, *J. Geophys. Res.*, 108, 4717,
12 2003.

13 Nieminen, T., Yli-Juuti, T., Manninen, H. E., Petäjä, T., Kerminen, V.-M., and Kulmala, M.:
14 Technical note: New particle formation event forecasts during PEGASOS-Zeppelin Northern
15 mission 2013 in Hyytiälä, Finland, *Atmos. Chem. Phys.*, 15, 12385–12396, doi:10.5194/acp-
16 15-12385-2015, 2015.

17 Nilsson, E. D., Rannik, Ü., Kulmala, M., Buzorius, G., and O’Dowd, C.: Effects of the
18 continental boundary layer evolution, convection, turbulence and entrainment on aerosol
19 formation, *Tellus*, 53B, 441–461, 2001a.

20 Nilsson, E. D., Paatero, J., and Boy, M.: Effects of air masses and synoptic weather on aerosol
21 formation in the continental boundary layer, *Tellus*, 53B, 462–478, 2001b.

22 Riccobono, F., Schobesberger, S., Scott, C. E., Dommen, J., Ortega, I. K., Rondo, L., Almeida,
23 J., Amorim, A., Bianchi, F., Breitenlechner, M., David, A., Downard, A., Dunne, E. M.,
24 Duplissy, J., Ehrhart, S., Flagan, R. C., Franchin, A., Hansel, A., Junninen, H., Kajos, M.,
25 Keskinen, H., Kupc, A., Kürten, A., Kvashin, A. N., Laaksonen, A., Lehtipalo, K., Makhmutov,
26 V., Mathot, S., Nieminen, T., Onnela, A., Petäjä, T., Praplan, A. P., Santos, F. D., Schallhart,
27 S., Seinfeld, J. H., Sipilä, M., Spracklen, D. V., Stozhkov, Y., Stratmann, F., Tomé, A.,
28 Tsagkogeorgas, G., Vaattovaara, P., Viisanen, Y., Vrtala, A., Wagner, P. E., Weingartner, E.,
29 Wex, H., Wimmer, D., Carslaw, K. S., Curtius, J., Donahue, N. M., Kirkby, J., Kulmala, M.,
30 Worsnop, D. R., and Baltensperger, U.: Oxidation Products of Biogenic Emissions Contribute
31 to Nucleation of Atmospheric Particles, *Science*, 344, 717–721, 2014.

1 Rose, C., Sellegri, K., Asmi, E., Hervo, M., Freney, E., Colomb, A., Junninen, H., Duplissy, J.,
2 Sipilä, M., Kontkanen, J., Lehtipalo, K., and Kulmala, M.: Major contribution of neutral
3 clusters to new particle formation at the interface between the boundary layer and the free
4 troposphere, *Atmos. Chem. Phys.*, 15, 3413–3428, doi:10.5194/acp-15-3413-2015, 2015.

5 Schobesberger, S., Junninen, H., Bianchi, F., Lonn, G., Ehn, M., Lehtipalo, K., Dommen, J.,
6 Ehrhart, S., Ortega, I. K., Franchin, A., Nieminen, T., Riccobono, F., Hutterli, M., Duplissy, J.,
7 Almeida, J., Amorim, A., Breitenlechner, M., Downard, A. J., Dunne, E. M., Flagan, R. C.,
8 Kajos, M., Keskinen, H., Kirkby, J., Kupc, A., Kuerten, A., Kurten, T., Laaksonen, A., Mathot,
9 S., Onnela, A., Praplan, A. P., Rondo, L., Santos, F. D., Schallhart, S., Schnitzhofer, R., Sipila,
10 M., Tome, A., Tsagkogeorgas, G., Vehkamäki, H., Wimmer, D., Baltensperger, U., Carslaw,
11 K. S., Curtius, J., Hansel, A., Petaja, T., Kulmala, M., Donahue, N. M., and Worsnop, D. R.:
12 Molecular understanding of atmospheric particle formation from sulfuric acid and large
13 oxidized organic molecules, *P. Natl. Acad. Sci. USA*, 110, 17223–17228, 2013.

14 Sipilä, M., Berndt, T., Petäjä, T., Brus, D., Vanhanen, J., Stratmann, F., Patokoski, J., Mauldin,
15 R. L., Hyvärinen, A.-P., Lihavainen, H. and Kulmala, M.: The role of sulfuric acid in
16 atmospheric nucleation, *Science*, 327 (5970), 1243–1246, 2010.

17 Sogacheva, L., Hamed, A., Facchini, M. C., Kulmala, M., and Laaksonen, A.: Relation of air
18 mass history to nucleation events in Po Valley, Italy, using back trajectories analysis, *Atmos.*
19 *Chem. Phys.*, 7, 839–853, doi:10.5194/acp-7-839-2007, 2007.

20 Spracklen, D. V., Carslaw, K. S., Kulmala, M., Kerminen, V.-M., Mann, G. W., and Sihto, S.-
21 L.: The contribution of boundary layer nucleation events to total particle concentrations on
22 regional and global scales, *Atmos. Chem. Phys.*, 6, 5631–5648, doi:10.5194/acp-6-5631-2006,
23 2006.

24 Tammet, H. and Kulmala, M.: Simulation tool for atmospheric aerosol nucleation bursts, *J.*
25 *Aerosol Sci.*, 36(2), 173–196, 2005.

26 Wang, M. and Penner, J. E.: Aerosol indirect forcing in a global model with particle nucleation,
27 *Atmos. Chem. Phys.*, 9, 239–260, doi:10.5194/acp-9-239-2009, 2009.

28 Vanhanen, J., Mikkilä, J., Lehtipalo, K., Sipilä, M., Manninen, H. E., Siivola, E., Petäjä, T., and
29 Kulmala, M.: Particle size magnifier for nano-CN detection, *Aerosol Sci. Tech.*, 45, 533–542,
30 2011.

1 Weber, R. J., Marti, J. J., McMurry, P. H., Eisele, F. L., Tanner, D. J., and Jefferson, A.:
2 Measurements of new particle formation and ultrafine particle growth rates at a clean
3 continental site, *J. Geophys. Res.*, 102, 4375–4385, 1997.

4 Wimmer, D., Lehtipalo, K., Franchin, A., Kangasluoma, J., Kreissl, F., Kürten, A., Kupc, A.,
5 Metzger, A., Mikkilä, J., Petäjä, T., Riccobono, F., Vanhanen, J., Kulmala, M., and Curtius, J.:
6 Performance of diethylene glycol-based particle counters in the sub-3 nm size range, *Atmos.*
7 *Meas. Tech.*, 6, 1793-1804, doi:10.5194/amt-6-1793-2013, 2013.

8 Winkler, P. M., Steiner, G., Vrtala, A., Vehkamäki, H., Noppel, M., Lehtinen, K. E. J., Reischl,
9 G. P., Wagner, P. E., and Kulmala, M.: Heterogeneous nucleation experiments bridging the
10 scale from molecular ion clusters to nanoparticles, *Science*, 319, 1374–1377,
11 doi:10.1126/science.1149034, 2008.

12 Yli-Juuti, T., Nieminen, T., Hirsikko, A., Aalto, P. P., Asmi, E., Hörrak, U., Manninen, H. E.,
13 Patokoski, J., Dal Maso, M., Petäjä, T., Rinne, J., Kulmala, M., and Riipinen, I.: Growth rates
14 of nucleation mode particles in Hyytiälä during 2003–2009: variation with particle size, season,
15 data analysis method and ambient conditions, *Atmos. Chem. Phys.*, 11, 12865-12886,
16 doi:10.5194/acp-11-12865-2011, 2011.

17 Yu, F. and Turco R.: Ultrafine aerosol formation via ionmediated nucleation, *Geophys. Res.*
18 *Lett.*, 27, 883–886, 2000.

19 Yu, F. and Turco, R.: Case studies of particle formation events observed in boreal forests:
20 implications for nucleation mechanisms, *Atmos. Chem. Phys.*, 8, 6085–6102, doi:10.5194/acp-
21 8-6085-2008, 2008.

22 Yu, F., Luo, G., Bates, T. S., Anderson, B., Clarke, A., Kapustin, V., Yantosca, R. M., Wang,
23 Y., and Wu, S.: Spatial distributions of particle number concentrations in the global
24 troposphere: Simulations, observations, and implications for nucleation mechanisms, *J.*
25 *Geophys. Res.*, 115, D17205, doi:10.1029/2009JD013473, 2010.

26 Yu, H., Kanawade, V. P., You, Y., Hallar, A. G., Mccubbin, I. B., Chirokova, G., Sedlacek, A.
27 J., Springston, S. R., Wang, J., Mc-Graw, R. L., Mikkila, J., and Lee, S. H.: Sub-3 nm particles
28 observed at the coastal and continental sites in the United States, *J. Geophys. Res. Atmos.*, 119,
29 doi:10.1002/2013JD020841, 2014.

- 1 Yu, H., Zhou, L. Y., Dai, L., Shen, W. C., Zheng, J., Ma, Y., and Chen, M. D.: Nucleation and
2 growth of sub-3 nm particles in the polluted urban atmosphere of a megacity in China, *Atmos.*
3 *Chem. Phys. Discuss.*, 15, 18653-18690, doi:10.5194/acpd-15-18653-2015, 2015.
- 4 Xiao, S., Wang, M. Y., Yao, L., Kulmala, M., Zhou, B., Yang, X., Chen, J. M., Wang, D. F.,
5 Fu, Q. Y., Worsnop, D. R., and Wang, L.: Strong atmospheric new particle formation in winter
6 in urban Shanghai, China, *Atmos. Chem. Phys.*, 15, 1769-1781, doi:10.5194/acp-15-1769-
7 2015, 2015.
- 8 Zhang, R., Khalizov, A., Wang, L., Hu, M., and Xu, W.: Nucleation and Growth of
9 Nanoparticles in the Atmosphere. *Chem. Rev e.*, 112, 1957–2011, 2012.
- 10

1 **Table 1:** Growth rates of particles during NPF events. The median values and the range from
2 5- to 95-percentile are shown. The growth rates were determined from the positive ion size
3 distributions measured with the NAIS.

4

Size range	Growth rate [nm h⁻¹]
1.5–3.0 nm	4.3 (1.0–10.0)
3.0–7.0 nm	6.0 (2.6–12.9)
7.0–20.0 nm	7.2 (3.8–13.8)

5

6

1 **Table 2:** The formation rates of all clusters and ions during NPF events. The median values
 2 and the range from 5- to 95-percentile are shown. The formation rates of all clusters at 1.6 nm
 3 were determined from PSM data. The formation rates of ions at 1.6 nm and all clusters and ions
 4 at 2 nm were determined from NAIS data.

Size	Clusters	Formation rate [$\text{cm}^{-3} \text{s}^{-1}$]
1.6 nm	All clusters	45 (23–53)
1.6 nm	Positive ions	0.19 (0.09–0.32)
1.6 nm	Negative ions	0.06 (0.03–0.08)
2.0 nm	All clusters	6.8 (2.7–38.5)
2.0 nm	Positive ions	0.12 (0.05–0.25)
2.0 nm	Negative ions	0.08 (0.03–0.19)

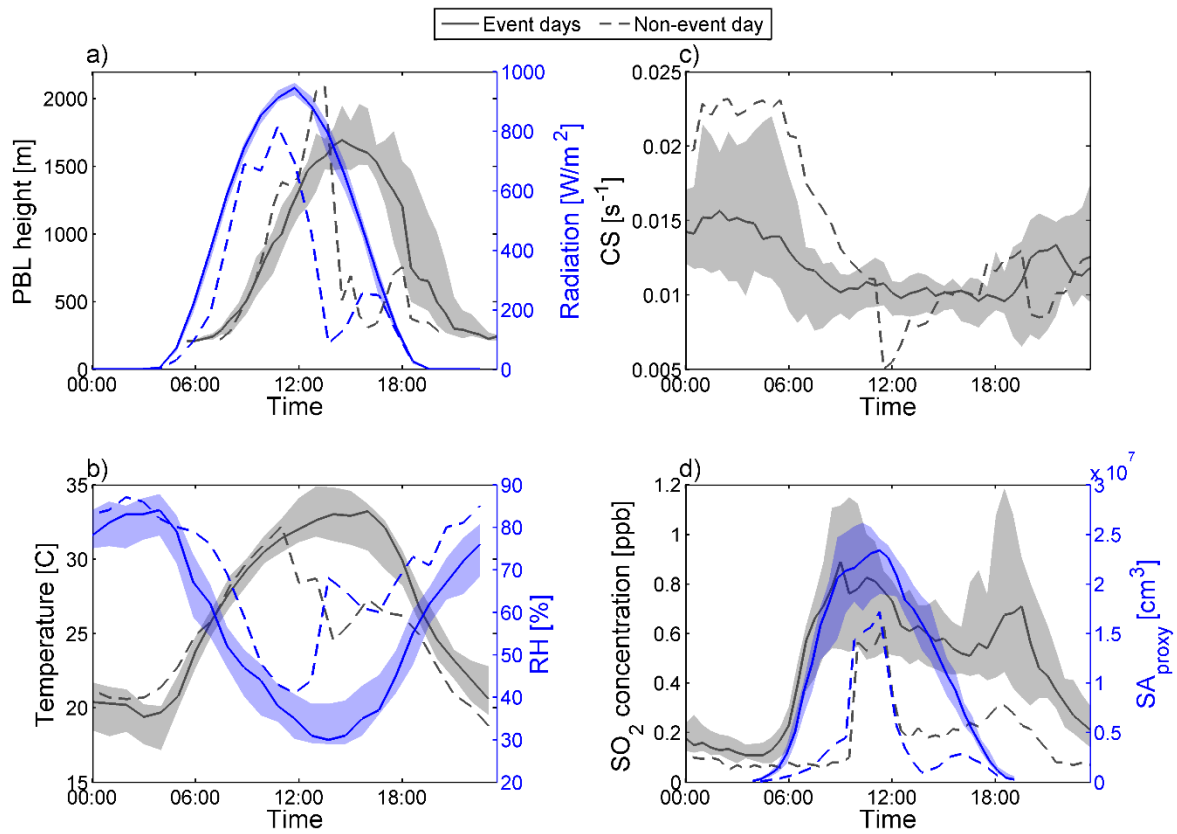
5

6



1
2
3
4
5
6
7

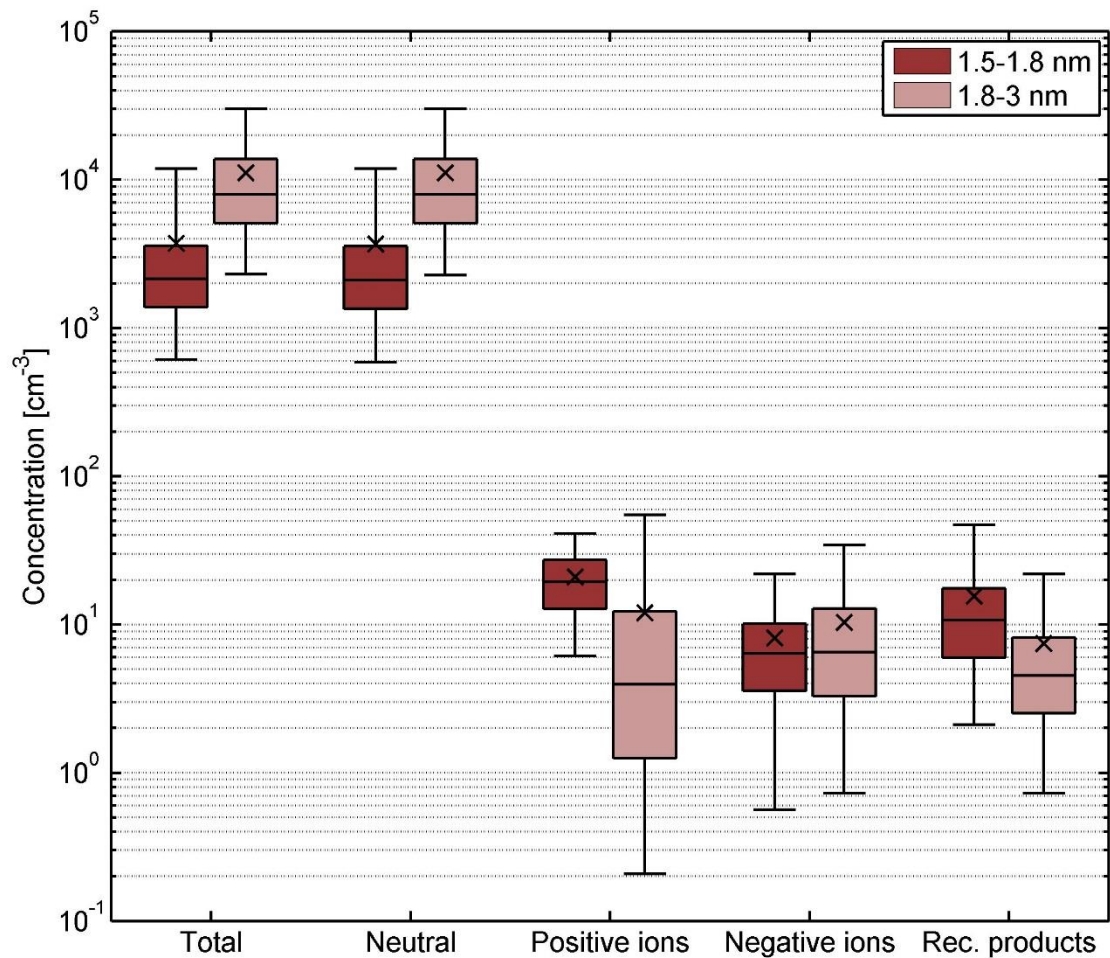
Figure 1: The map of Northern Italy, where the location of the San Pietro Capofiume (SPC) measurement site is shown with a red marker. Map data provided by Google.



1

2 **Figure 2:** The diurnal variation of different variables during the measurement campaign: a)
 3 PBL height (grey) and global radiation (blue), b) temperature (grey) and relative humidity (RH;
 4 blue), c) condensation sink (CS), d) SO₂ concentration (grey) and sulfuric acid proxy (SA_{proxy};
 5 blue). The median diurnal pattern on NPF event days is shown as solid lines, and the 25% to
 6 75% percentile range as the shaded area. The diurnal variation on the only non-event day (6
 7 July 2012) is shown as dashed lines. Time is UTC + 1 h.

8

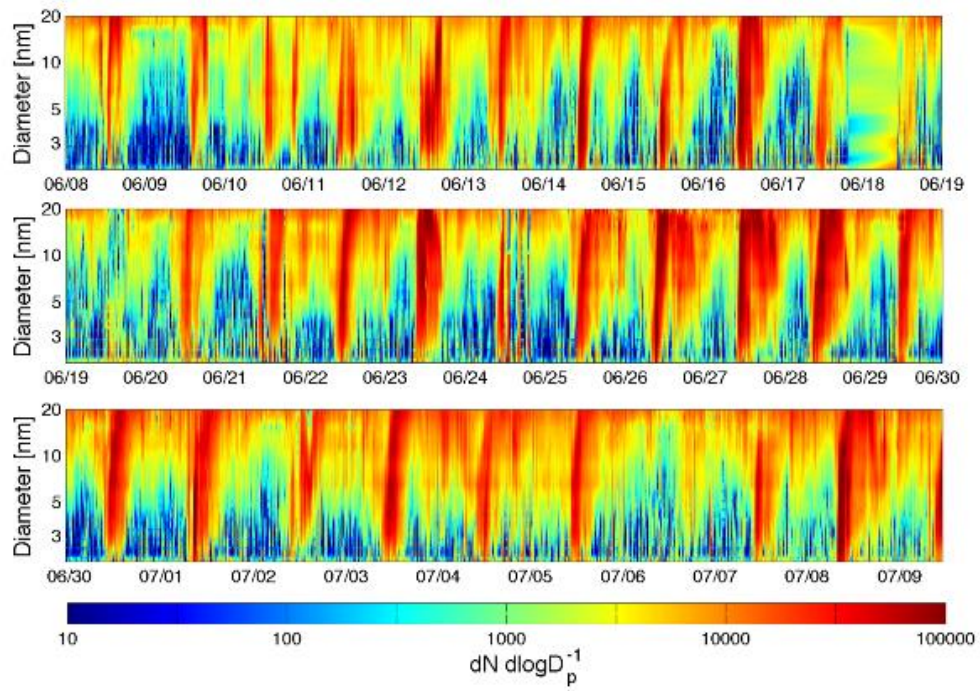


1

2 **Figure 3:** The median concentration of all clusters, neutral clusters, positive ions, negative ions
 3 and recombination products in the two size bins (1.5–1.8 nm and 1.8–3.0 nm). The edges of the
 4 boxes show the 25- and 75-percentiles and the centers of the boxes represent the median values.
 5 The mean values are presented with black crosses. The error bars show the 5- and 95-percentile
 6 values.

7

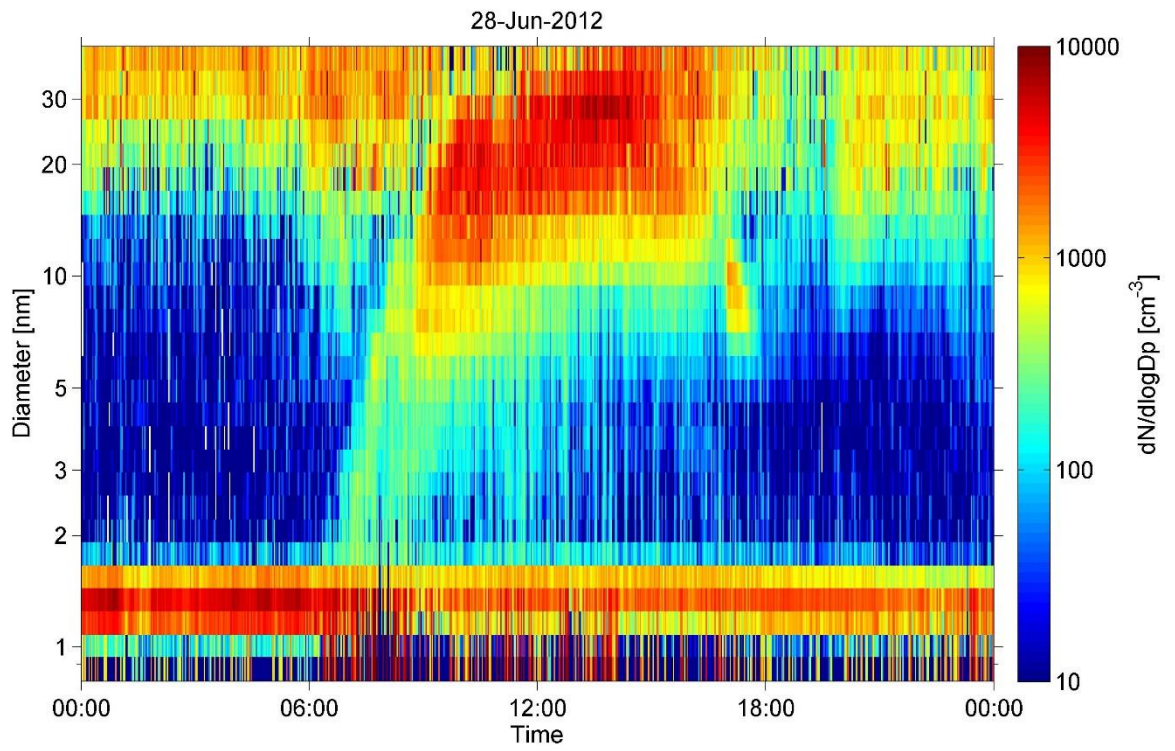
8



1

2 **Figure 4:** Time series of particle size distribution measured with the NAIS during 8 June – 9
 3 July 2012 in San Pietro Capofiume.

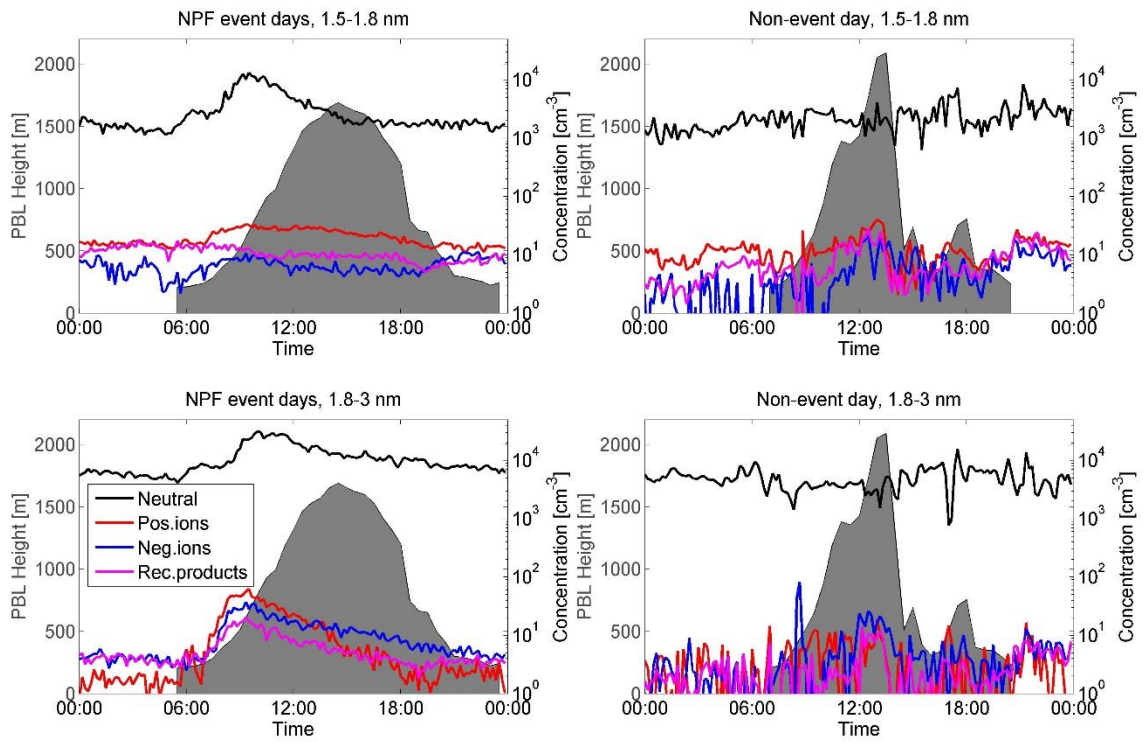
4



1

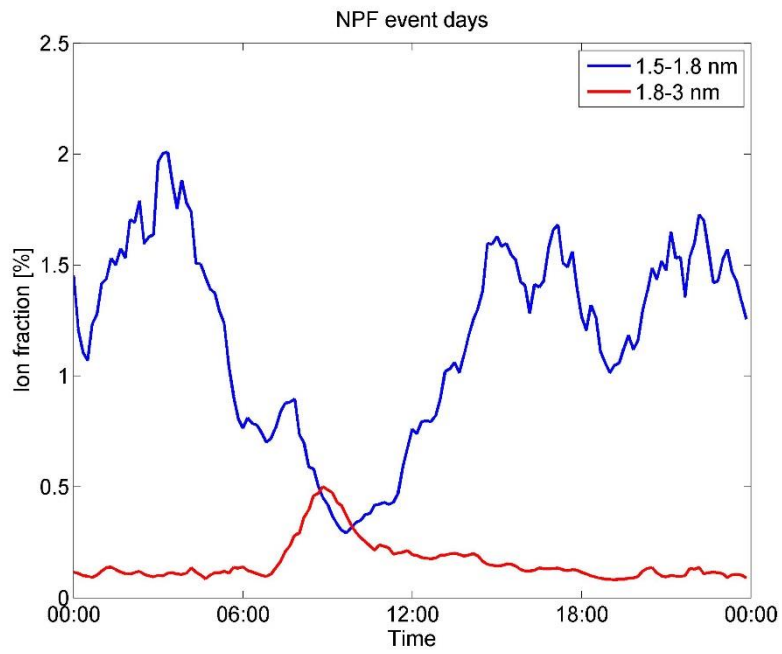
2 **Figure 5:** The size distribution of positive ions on a typical new particle formation event at the
3 San Pietro Capofiume station (28 June 2012).

4



1
2
3
4
5
6

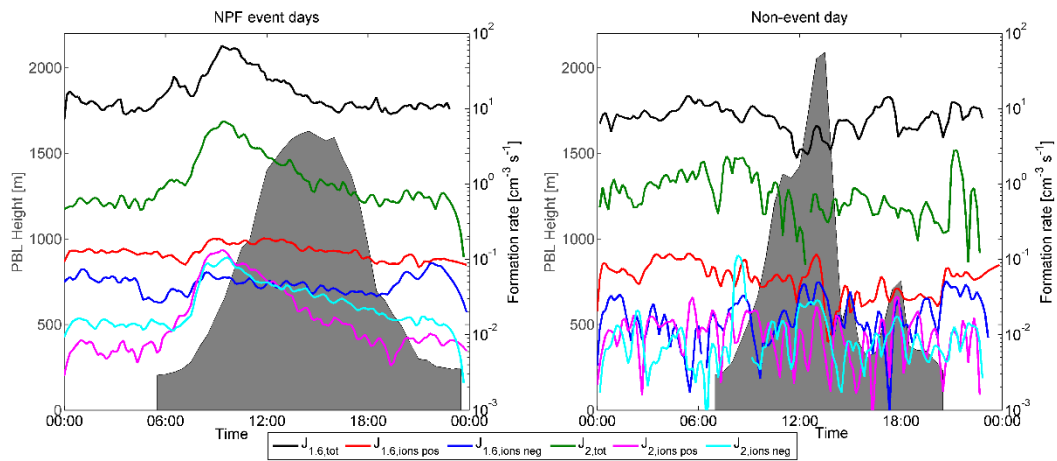
Figure 6: The median diurnal variation of the concentrations of neutral clusters (black line), positive ions (red line), negative ions (blue line) and recombination products (magenta line) on NPF event days and on the only non-event day (6 July 2012). In addition, the PBL height is shown in grey. Time is UTC + 1 h.



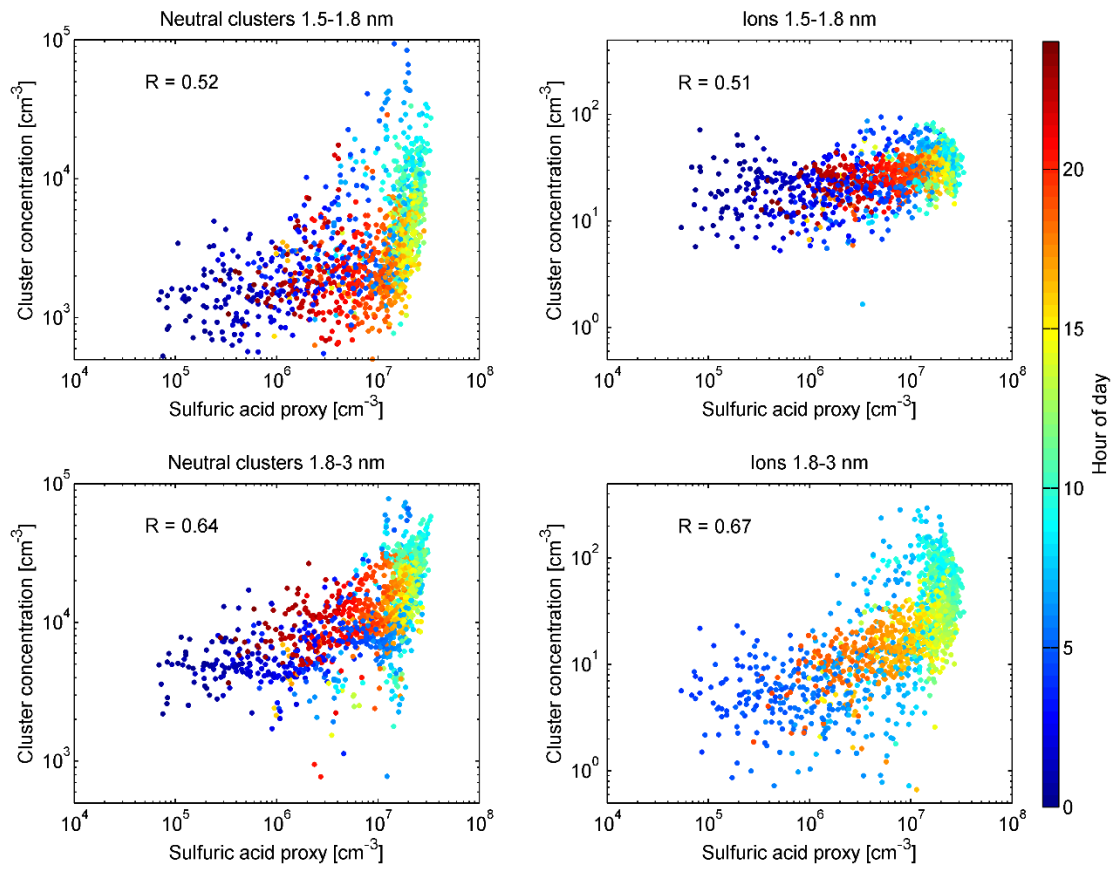
1

2 **Figure 7:** The median diurnal variation of the fraction of ions of all clusters in the size bins of
3 1.5–1.8 nm (blue line) and 1.8–3.0 nm (red line) on NPF event days. Time is UTC + 1 h.

4



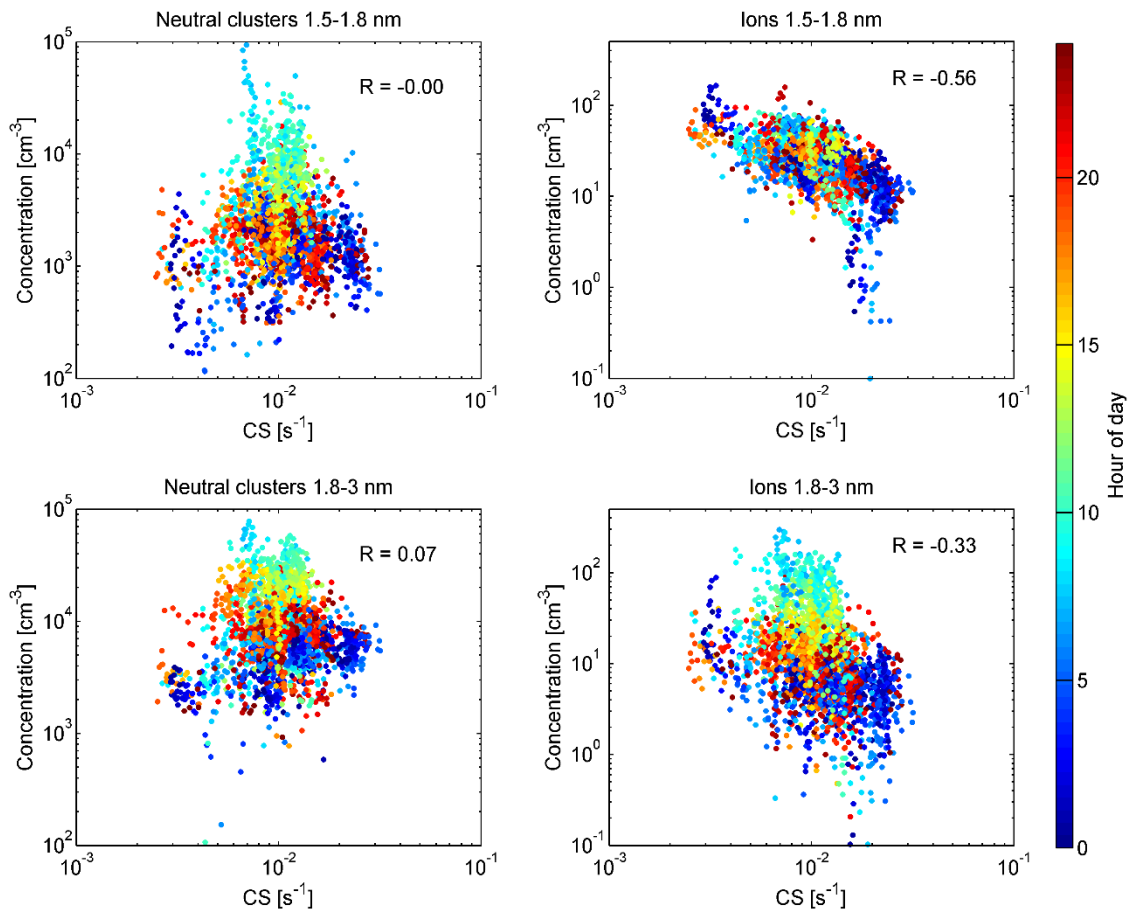
1
 2 **Figure 8:** The median diurnal variation of the cluster formation rates at 1.6 nm and 2 nm on
 3 NPF event days and on the only non-event day (6 July 2012). The PBL height is shown in grey.
 4 In the subscripts numbers refer to the size of the cluster in nanometers and “tot” refers to total
 5 clusters, “pos” to positive ions and “neg” to negative ions. Time is UTC + 1 h.
 6



1

2 **Figure 9:** The correlation between the neutral and charged 1.5–1.8 nm and 1.8–3.0 nm clusters
 3 and sulfuric acid proxy. The color bar shows the hour of day. The correlation coefficients (R)
 4 are presented in the figures.

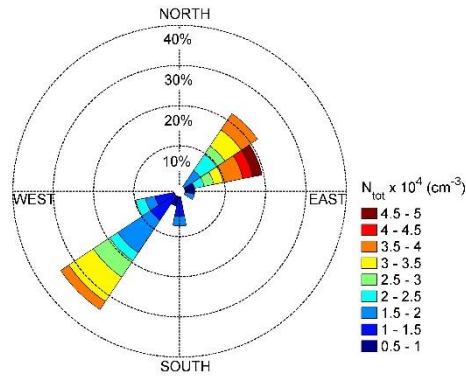
5



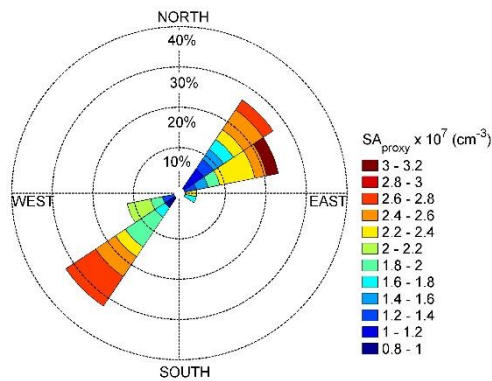
1

2 **Figure 10:** The correlation between the neutral and charged 1.5–1.8 nm and 1.8–3.0 nm clusters
 3 and condensation sink (CS). The color bar shows the hour of day. The correlation coefficients
 4 (R) are presented in the figures.

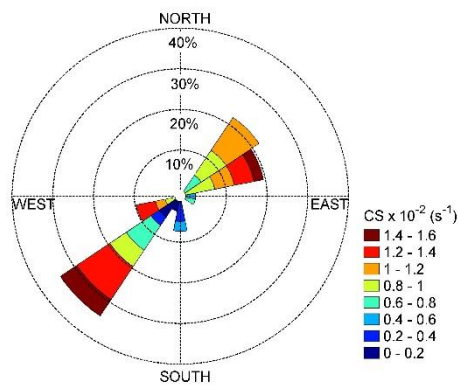
5



1



2



3

4 **Figure 11:** Air mass arrival directions and their relation to the total concentration of 1.8–3.0
 5 nm clusters (N_{tot}), sulfuric acid proxy (SA_{proxy}) and condensation sink (CS) in San Pietro
 6 Capofiume around midday (between 10 a.m. and 2 p.m.). The length of the sectors illustrates
 7 how frequently an air mass trajectory arrived from that direction. The color of the sectors shows
 8 the value of the measured variable in San Pietro Capofiume at the arrival time of the trajectory.